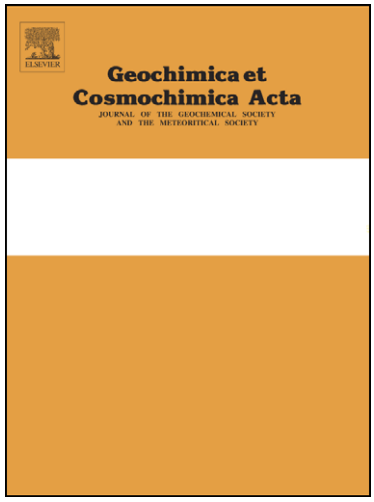

Hydrothermal fluid evolution and metal transport in the Kiruna District, Sweden: Contrasting metal behaviour in aqueous and aqueous-carbonic brines

M.P. Smith, S.A. Gleeson, B.W.D. Yardley

PII: S0016-7037(12)00591-1
DOI: http://dx.doi.org/10.1016/j.gca.2012.10.015
Reference: GCA 7960

To appear in: *Geochimica et Cosmochimica Acta*

Received Date: 27 April 2012
Accepted Date: 9 October 2012

Please cite this article as: Smith, M.P., Gleeson, S.A., Yardley, B.W.D., Hydrothermal fluid evolution and metal transport in the Kiruna District, Sweden: Contrasting metal behaviour in aqueous and aqueous-carbonic brines, *Geochimica et Cosmochimica Acta* (2012), doi: http://dx.doi.org/10.1016/j.gca.2012.10.015

Hydrothermal fluid evolution and metal transport in the Kiruna District, Sweden: Contrasting metal behaviour in aqueous and aqueous-carbonic brines.

M.P. Smith[1*], S.A. Gleeson[2] and B.W.D. Yardley[3].

1. School of Environment and Technology, University of Brighton, Brighton, BN2 4GJ, U.K.
2. Department of Earth & Atmospheric Sciences, University of Alberta, Edmonton, AB, T6G 2E3, Canada
3. School of Earth and Environment, University of Leeds, Leeds, LS2 9JT, U.K.

*Corresponding author:
Dr. Martin Smith,
School of Environment and Technology,
University of Brighton,
Lewes Road,
Brighton,
BN2 4GJ.
U.K.

e-mail: martin.smith@brighton.ac.uk
Tel.: (+44)(0)1273 642265

Abstract

Iron oxide-copper-gold (IOCG) deposits and Fe oxide-apatite deposits from Norrbotten, Sweden, formed in similar settings, and in some cases IOCG mineralisation overprinted Fe oxide-apatite mineralisation. Fluid inclusions in quartz veins cutting Fe oxide-apatite deposits range in salinity from 33-37 wt. % NaCl eq., and those in IOCG-type deposits from 41-54 wt. % NaCl eq. Minimum trapping conditions for these inclusions are ~200-300MPa and 200-300°C in the Fe oxide-apatite bodies, and 250->300MPa and 300-500°C in the IOCG deposits. Deformed Cu-Au deposits have similar early fluid characteristics, but contain complex secondary fluid inclusion assemblages including halite saturated (20-30 wt. % NaCl eq.), aqueous-carbonic (3-13 wt. % NaCl eq.; $X(CO_2)$ 0.17-0.29) and CO_2-rich fluids. The aqueous-carbonic and carbonic inclusions are consistent with aqueous-carbonic fluid immiscibility at ~150MPa. A secondary population, with a high Ca-content occurs in all deposit types.

The chemical composition of these inclusions has been determined by crush-leach analysis and LA-ICPMS. Halogen contents indicate a range of salinity sources with possible inputs from both magmatic and halite-dissolution brines. Element ratios suggest the alkali content of the fluid exceeded the buffer capacity of the host rocks. Iron and other transition metal contents correlate strongly with Cl concentrations, with secondary controls on solubility from pH, redox and temperature. Copper and Ag contents are higher in lower salinity aqueous-carbonic brines (up to 5000ppm Cu, 900ppm Ag) than in the most saline brines (up to 2297ppm Cu, 837ppm Ag). This may reflect differences in metal source between deposit types, but is also consistent with the complexation of Cu by bisulphide in the lower salinity fluids. Late stage

aqueous-carbonic fluid flux through the deformed deposits either introduced additional copper to the deposits, remobilised pre-existing copper or both.

1. Introduction

Iron oxide–copper–gold deposits (IOCG) are a relatively recently defined class of ore deposit, which are characterised by Cu-sulphide ± Au hydrothermal ores with abundant magnetite or hematite. Their classification has been problematical since the definition of the Fe oxide-Cu-Au (IOCG) class of deposits by Hitzman (1992). Subsequent research has refined the definition (Hitzman, 2000; Williams et al., 2005; Groves et al., 2010), and suggested the Fe oxide-apatite (Kiruna-type) deposits are a separate, but related, type of ore deposit. A range of genetic models have also been proposed for IOCG deposits that have included the involvement of basinal brines, fluids interacted with meta-evaporites, surface derived brines (e.g. Barton and Johnson, 1996; 2000) and magmatic fluids in ore formation. Evidence from different deposits and districts supports the potential involvement of all these fluid sources in producing deposits of similar characteristics (e.g. Williams et al., 2001; Kendrick et al., 2007, 2008a, b; Gleeson and Smith, 2009). The key linking factor in all models is the involvement of high salinity brines, which account for the high total masses of Fe deposited and the prevalence of Na-rich alteration including the formation of regional scapolite and albite. There is also good evidence for mixing of different fluids, and/or for numerous generations of fluid circulation (Broman and Martinsson, 2000; Wanhainen et al., 2003; Gleeson and Smith, 2009), including CO_2-rich fluids either during the main stage of ore deposition, or involved in post ore modification of the deposits (e.g. Williams et al., 2001; Fu et al., 2003; Baker et al., 2008). In many instances in IOCG deposits Cu-(Au) mineralisation post-dates Fe mineralisation, with

Cu minerals either in cross-cutting veins or in breccia matrices, and may be the result of the circulation of different fluids through the same deposit with a significant time difference between the mineralising events (e.g. Smith et al., 2009). However, despite the complex interaction of primary fluid sources, fluid mixing, immiscibility and multiple generations of overprint, studies so far that have targeted the chemistry of individual fluid inclusions have found the highest concentrations of ore forming elements, particularly Cu, in high temperature, hypersaline fluids of inferred to be of either magmatic derivation (Baker et al., 2008), or non-magmatic brines(Bastrakov et al., 2007). Even in deposits with primary fluids suggested to be of magmatic origin, however, there is evidence for the subsequent interaction of evaporate-derived brines (Baker et al., 2008).

In this study, we report on the characteristics of aqueous and aqueous-carbonic fluid inclusions from quartz veins cutting Fe oxide-apatite mineralisation, and hosting Cu mineralisation in IOCG deposits, from the Kiruna and Malmberget ore districts, northern Sweden (Fig. 1) with the aims of examining the formation conditions of the veins and ores and the transport and deposition processes of metals. The study used crush leach and laser ablation Inductively Coupled Plasma Mass Spectrometry (LA-ICPMS) analyses of fluid inclusion chemistry to give constraints on both the cation and anion composition of fluids, and to allow discrimination between different populations in mixed inclusion assemblages where crush leach techniques would average the chemistry of different populations.

2. Background geology

The detailed geology and metallogeny of Norrbotten County, Sweden, have been reviewed by Carlon (2000) and Bergman et al. (2001). Fe oxide-apatite and

IOCG type deposits are hosted in a Palaeoproterozoic sequence of metavolcanic and metasedimentary rocks, that can be broadly divided into the Karelian Greenstone Group (>1.9Ga) and the Svecofennian Porphyry Group (Fig. 1). The Greenstone Group consists of dominantly tholeiitic to komatiitic volcanic rocks, and overlies Archaean basement (Ekdhal, 1993). The Porphyry Group consists of andesitic (Porphyrite Group) to syenitic and quartz-syenitic (Kiruna Porphyries) igneous rocks and associated sediments (Martinsson, 1997). The Kiruna Porphyries host the Kiirunavaara magnetite-apatite deposit, and may have acquired their syenitic character by metasomatism, and the porphyry group has been identified as initially consisting of a sequence of basalt, trachyandesite and rhyodacite-rhyoite (Martinsson and Perdahl, 1995; Bergman e al., 2001). Storey et al. (2007) suggested a minimum formation age for these units of ca. 2050Ma. These rocks are cut by the calc-alkaline Haparanda and Perthite-Monzonite granitoid suites (1.9-1.8Ga; Skiöld, 1987), followed by the Lina suite granitoids at around 1.79Ga. The country rocks underwent metamorphism, peaking at upper greenschist to lower amphibolites facies conditions from 1.9-1.8Ga (Skiöld, 1987). The rocks are affected by albitisation and scapolitisation on the regional scale (Frietsch et al., 1997), which occurred at ~1903±8Ma (Smith et al., 2009). A number of large-scale shear systems cut the area, including the Nautanen Deformation Zone (NDZ), a NNW-trending structure with schistose or mylonitic rocks occurring in several high strain branches in a zone up to 3km wide (Martinsson and Wanhainen, 2004).

Samples for this study were taken from three groups of deposits and prospects; late-stage quartz veins cutting Fe oxide-apatite deposits and associated alteration, mineralization-related quartz veins from Cu-(Au) prospects hosted by the Greenstone

and Porphyry Groups, and mineralization-related quartz veins from the heavily deformed metavolcanic rocks of the NDZ. The Fe oxide- apatite bodies are typified by the Kiirunavaara-Luossavaara body, dominated by magnetite, and the Per Geiger ores, with both hematite and magnetite (Geijer, 1910; Martinsson, 2004). The formation of the Kiirunavaara-Luossavaara ores has been dated at 1880-1870Ma (Romer et al., 1994; Smith et al., 2009), which is coeval with both the intrusion of the Haparanda and Perthite-Monzonite suite granitoids, and peak metamorphic conditions in the area (Bergstrom et al., 2001), although the ores underwent a second period of metamorphism and possibly hydrothermal alteration at ~1800Ma (Romer et al., 1994; Smith et al., 2009). Quartz veins cross-cut magnetite and/or hematite in these deposits (Fig. 2A, B) and so cannot be directly linked to ore deposition. However, the quartz veins also include actinolite, magnetite, hematite and titanite (Fig. 2A, B), and do not show alteration haloes when cross-cutting oxide ore (there is no hematisation of magnetite; Fig. 2C). We therefore argue that these veins represent the latest stage fluid associated with the main stage of Fe oxide deposition, and hence have provide some constraints on the transport of metals in these systems. Hematite-bearing veins do occur, and are represented in this study by the late stage quartz vein sample from Kirunavaara (KR2), and veins from the Nuktus deposit.

The IOCG deposits occur in both Greenstone Group and Porphyry Group rocks affected by sodic , (including both scapolite and albite), potassic and carbonate alteration (Martinsson, 2004). It is likely that IOCG mineralisation post-dated Fe oxide-apatite mineralisation by 10-20Ma (Martinsson and Virkkunen, 2004; Smith et al., 2009). In these deposits quartz veins host chalcopyrite and pyrite, and so the deposition of quartz can be closely related to ore mineral deposition (Fig. 2D, E).

Quartz veins directly associated with Cu mineralisation were also taken from sites associated with the NDZ, where shear-zone hosted mineralisation is associated with the development of scapolite, tourmaline, sericite, K-feldspar, epidote and garnet (Martinsson and Wanhainen, 2004). The samples come from both the Nautanen prospect, and from the Ferrum vein hosted Cu-Au prospect on the margins of the main deformation zone. An additional sample from the Aitik Cu-Au mine (Wanhainen et al., 2003) was analysed for comparison with the Nautanen samples. It has been suggested that primary mineralisation in the NDZ was formed at a similar time to other mineralisation in the area (1870-1890Ma; Wanhainen and Martinsson, 2003; Wanhainen et al., 2005), although the Aitik deposit may represent a deformed and metamorphosed porphyry-Cu system (Monro, 1988). The ore mineral assemblage in both deposits is typified by pyrite, chalcopyrite, magnetite and pyrrhotite (Fig. 2F). Both the Nautanen prospect and Aitik deposit were significantly modified, and ore metals remobilised by subsequent deformation and metamorphic events associated with the formation of the deformation zone, notably at ~1760Ma (Wanhainen et al., 2005; Smith et al., 2009). Secondary fluid inclusions can be related to either remobilisation of Cu or addition of Cu to the deposits as sulphides phases occur as solid inclusions along secondary fluid inclusion trails (Wanhainen et al., 2003).

The settings and characteristics of individual samples are described in Table 1, and additional descriptions of the same samples are given by Gleeson and Smith (2009).

*3. Methods

3.1 Fluid inclusion microthermometry

Inclusions were classified as primary, pseudosecondary or secondary using the criteria of Roedder (1984), and using their room temperature phase assemblage (Lw – liquid water; Lc – carbonic liquid; V – vapour; Sh – solid halite; nS – multiple solids). Microthermometric data were collected using a Linkam THMSG 600 heating and freezing stage which was calibrated at -56.6ºC, 0ºC, and 10ºC using synthetic fluid inclusion standards and distilled water, and at high temperatures using a range of pure solids. All measurements were made during heating runs to avoid problems of metastability. At low temperatures (<30°C) heating rates of 0.5°C/min were used, with a precision of ±0.2ºC, and rates of 5°C/min, with a precision of ±1ºC for measurements of solid dissolution and liquid-vapour homogenisation temperature (T_h). Key samples were photographed and inclusion locations accurately mapped for location for subsequent LA-ICPMS analysis of inclusion chemistry.

Fluid inclusion salinities were calculated as weight % NaCl equivalent (wt. % NaCl eq.) directly from halite dissolution (Sterner et al., 1988), from ice melting temperatures (Bodnar, 1993), and from clathrate melting in the Q2 assemblage (Lw+Lc+V+Clathrate; Diamond, 1990). Where possible NaCl:$CaCl_2$ ratios where estimated using the ice melting temperature and the halite dissolution temperature (for halite saturated inclusions; Williams-Jones and Samson, 1990), and the hydrohalite melting temperature (for halite undersaturated inclusions; Oakes et al. 1990) . The composition of Lw+Lc+V inclusions was calculated from T_hCO_2,, salinity calculated from T_mClath and estimated volume proportions of the gas phase using the BULK program (Bakker, 2003) using the Archer (1992) ion interaction model and the gas-fluid-salt mixing model of Krumgalz et al. (1996). Isochores for all inclusions except Lw+Sh+V inclusions were calculated using the ISOC program (Bakker, 2003) and the equations of state for the NaCl-CO_2-H_2O system of Bowers and Helgeson (1983), for

the system NaCl-$CaCl_2$-H_2O of Zhang & Frantz (1987), and the pure CO_2 system of Span & Wagner (1996). The position of the halite solidus and estimates of pressure at homogenisation from Lw+Sh+V inclusions were calculated using the equations of Bodnar (1994) and Becker et al., (2008). Estimates of the pressure at total homogenisation of Lw+Sh+V inclusions homogenising by halite dissolution are very approximate because many measurements are not covered by the experimental range of Becker et al., (2008). The bulk salinities calculated for these inclusions using the equation of Sterner et al. (1988) are also likely to be slightly under estimated (Bodnar, 1994; Becker et al., 2008), but the error on a calculated salinity is likely to be ≤1wt.% NaCl eq.

3.2 Crush-leach analysis

To produce enough leachate for major, minor and trace element analyses, quartz vein samples were cleaned and hand-picked to produce a total of 5g of material. The samples were then washed in 18.2 mΩ water and heated overnight on a hot plate, then dried in an oven. Two grams were crushed and leached in a clean environment using the technique described in Gleeson and Turner (2007). All the leachates were analysed by a DX600 ion chromatograph for Cl^-, Br^-, F^-, sulphate and phosphate, and for Na by atomic adsorption spectroscopy. Replicate analyses were within 2% for Cl^- and SO_4^{2-} and 5% for F^-, Br^- and Na^+. This leachate was also analysed for chlorine stable isotopes (Gleeson & Smith 2009). The second aliquot of sample was leached with a La-dosed solution and this was analysed by ICP-MS and atomic emission spectroscopy for Na, Ca, Fe, Mn, K, Mg, Pb, Zn, Sr, Ba, Al, Cu, B, Li, Co, As, Cd, Si, S, Sb, Be, Cr, Mo, Ni, Se Ag, Tl, Sn, Ti, U and V. Of these elements, Na, Ca, Fe, K, Pb, Zn, Sr, Ba, Al, Cu, B, Li, Co, As, Cd and Si were routinely detected in the samples. Analytical precision on these elements is typically within ±5%.

3.3 Laser Ablation ICP-MS

Fluid inclusions were analysed following the method of Allan et al. (2005) using a GeoLas Q Plus Excimer laser (ArF, 193nm, Microlas, Göttingen, Germany). Ablated material was transported from a cylindrical chamber with a height of 5 mm and internal diameter of 57 mm (approximately 13 cm^3) in 0.68 L/min He via Teflon® tubing to a cyclone gas mixer, where the analyte was premixed with 0.95 L/min Ar before introduction into the plasma. The analyte was analysed with an Agilent 7500c quadrupole ICP-MS, equipped with an octopole reaction cell that was pressurized with 2.5 mL/min H_2, which virtually eliminated $^{40}Ar^+$ and $^{40}Ar^{16}O^+$ interferences on $^{40}Ca^+$ and $^{56}Fe^+$, respectively, and greatly reduced the high Ar-based backgrounds on $^{39}K^+$. Fluid inclusion analyses were calibrated using combinations of NIST SRM 610 and 612, an in-house EMPA glass standard, and HNO_3 spiked aqueous standards ablated directly through the walls of glass capillaries (Ghazi and Shuttleworth, 2000; Günther et al., 1997; Boué-Bigne et al., 1999). Silicate glass standards were ablated for 200 pulses over a single 50 μm spot, using a repetition rate of 5 Hz and laser fluence of 10 J/cm^2. Laser focus on the ablation surface was maintained by raising the ablation cell 1μm per 10 shots, in accordance with an approximate ablation rate of 0.1 μm/pulse. Sodium was used as the internal standard in all cases. Sets of fluid inclusion analyses were bracketed by standards, and linear drift corrections were applied. Dwell times were 5 - 15 ms.

The absolute concentration of cations in analysed inclusions, and in bulk leachates was calculated by charge balance of the total cations against a Cl molality determined from microthermometric data wherever possible (Allen et al., 2005). An octopole reaction cell was not used for the analyses including Br and Cl to maximise the sensitivity on those elements, but this allowed polyatomic interferences on some

elements which were consequently omitted from the element list ($^{40}Ca^{+}$, $^{56}Fe^{+}$, $^{39}Ca^{+}$ - Allan et al., 2005). In the case of analyses of inclusions for Cl and Br therefore, where a limited element list was used, the element ratios from the analyses were normalised to the total Cl concentration in ppm. Limits of determination varied according to inclusion, and were defined as 6σ in the background counts. Signals below this limit were rejected *

4. Results

4.1 Fluid inclusion petrography

The petrography of fluid inclusions from the samples used here is described in Gleeson and Smith (2009) and is summarised briefly in Table 2 and Figure 3. In late stage quartz veins from the Fe oxide-apatite deposits, along with Lw+Sh+V (Fig. 3A) inclusions trapped on annealed trails, inclusions of consistent microthermometric properties occur in settings interpreted as primary, in growth zone parallel trails (Fig. 3B), or isolated in grain cores. Metastable Lw+Sh inclusions occur which nucleated a vapour bubble on freezing. The sample from the Henry Fe-oxide-apatite body is notable in that halite-bearing inclusions showed a double meniscus and a small amount of CO_2 within the inclusion (Fig. 3C). In Pahtohavare and other relatively undeformed IOCG deposits the inclusions (typically Lw+nS+V; Fig, 3D) are likewise trapped in primary settings, notably in vein wall parallel trails or as randomly distributed groups, overgrown by inclusion free rims (Fig. 3E, F). Secondary trails are dominated by CO_2-rich inclusions (Lindblom et al., 1996). The majority of samples from undeformed Fe oxide-apatite and IOCG deposits were analysed by crush-leach techniques, with selected samples from Kiruna, Nuktus and Pahtohavare also analysed by LA-ICPMS.

At Nautanen and other NDZ-related deposits all the inclusions analysed were trapped in annealed fractures. Halite-bearing inclusions can be divided into those that occupy discrete trails of a single inclusion phase assemblage, and those that form part of an assemblage with an Lw+Lc+V inclusion population. The highest salinity inclusions (Fig. 3G) are similar to those noted as primary in the Aitik deposit by Wanhainen et al., (2003). The inclusion assemblage from deposits associated with the NDZ includes coexisting Lc+V (Fig. 3H) Lw+Lc+V and Lw+Sh+V (Fig. 3I) inclusions. The Lw+Lc+V and Lc+V inclusions are in some instances preserved along the same secondary fluid inclusion trails (Fig. 3J) suggesting phase separation. These complex inclusion assemblages were targeted for LA-ICPMS analysis in order to investigate the chemistry of inclusions of contrasting room temperature phase assemblage within the same overall inclusion assemblage.

4.2 Microthermometry

The results of fluid inclusion microthermometry are summarised in Tables 2 and 3, and shown in Figure 4. In Lw+Sh+V inclusions in quartz veins from Fe oxide-apatite deposits first melting temperatures ranged from -68°C to -50°C, indicative of NaCl-bearing solutions containing a range of other monovalent and divalent cations (most likely including $CaCl_2$ and $FeCl_2$). The salinity of these inclusions, with the exception of a single sample from the Mertainen deposit (52 wt. % NaCl eq), varies from 30.4 to 41.2 weight % NaCl equivalent. Estimates of bulk salinity in the system NaCl-$CaCl_2$-H_2O range from 34 to 47 wt. % NaCl+$CaCl_2$ eq., with NaCl-$CaCl_2$ mass ratios from ~1 to 6 (Table 3; Fig. 4A). In the Lw+Lc+Sh+V inclusions from the Henry deposit clathrate melting was never observed, and decrepitation prior to total homogenisation (T_h) was common. Estimation of inclusion composition from

microthermometric data and estimates of phase volume proportions suggests salinities from 33 to 38 wt. % NaCl eq., with XCO_2 in the bulk inclusion ranging from 0.01 to 0.03. This sample also included a secondary population of Lw+Lc+V inclusions (Table 3) with compositions of ~21.5 wt. % NaCl eq. and XCO_2 ranging from 0.03 to 0.06.

Primary, pseudosecondary and secondary inclusions from relatively undeformed IOCG deposits are Lw+nS+V halite-bearing inclusions, with the main solid being halite. Microthermometric and laser Raman spectroscopic investigations by Lindblom et al. (1996) also identified sylvite, calcite, hematite and graphite in inclusions from Pahtohavare. Lw+Sh+V inclusions dominate in the sample from Kiskamavaara. Secondary trails of Lc+V inclusions are common. In most cases, salinities ranged from ~40 to ~58 wt. % NaCl eq. The fluids are NaCl dominated, with NaCl:$CaCl_2$ ratios ranging from ~6 to 21. Lw+Sh+V inclusions at Kallosalmi and Pahtohavare, Kiskamavaara, and Gruvberget range in salinity from ~30 to 38 wt. % NaCl eq (Table 3; Fig. 4B). The Lc+V inclusions have T_mCO_2 temperatures ranging from -56.6 to 60°C, indicating CO_2-dominated fluids. Lindblom et al. (1996) identified N_2 in addition to CO_2 in this inclusion type. Carbonic phase homogenisation was always to the liquid and ranged from -16 to 22°C. A secondary population of Lw+V inclusions was observed in samples from the Gruvberget deposit. These show $T_m$ice from -6.8 to -45 and $T_m$hh from -30 to -48°C, consistent with Ca-rich brines (Oakes et al., 1990; Table 3; Fig. 4B). This population has been noted from other deposits in the area (Broman and Martinsson, 2000; Wanhainen et al., 2003).

All samples analysed from deposits and prospects within or near the Nautanen Deformation Zone (NDZ) have complex fluid inclusion assemblages and parageneses

(Wanhainen et al., 2005). Halite-bearing inclusions in discrete trails have similarities to those observed in the Fe oxide-apatite deposits and the IOCG deposits (salinity from 31-52 wt. % NaCl eq. and T_hL-V from 138-196ºC; Table 3 Fig. 4C). Separate populations of Lw+Sh+V inclusions with salinity from 30 to 26 wt. % NaCl eq. and T_hL-V from ~120 to 180°C also occur. Secondary Lw+V inclusions have T_hL-V range from ~110 to 200°C, and fall into two broad compositional groups: a Ca dominated brine, with salinities from 22 to 33 wt. % NaCl eq. and NaCl:$CaCl_2$ ratios ranging from 0.2 to 0.5 and a more Na-rich fluid with salinities from 22 to 26 wt. % NaCl eq. (~20 to 24 wt % NaCl+$CaCl_2$ eq.) and NaCl:$CaCl_2$ ratios ranging from 0.5 to 1.3 (Table 3).

In samples from both Nautanen (NAU77006 210.47m) and Aitik (A3) more complex assemblages occur on individual trails (Fig. 3j) with trails noted with assemblages including [Lw+V plus Lw+Lc+V], [Lc+V plus Lw+V plus Lw+Sh+V], [Lw+V plus Lw+Lc+V plus Lw+Sh+V] and [Lw+Sh+V plus Lc+V]. These are shown in square brackets to highlight assemblages on individual planes. Care must be taken with both the Lw+V and Lc+V inclusions in these examples as these may have small amounts of either the carbonic phase of aqueous phase respectively as thin films that were not observed microscopically. Aqueous liquid plus halite plus vapour inclusions from these assemblages range in salinity from 28 to 35 wt. % NaCl eq. and homogenise between approximately 100 to 200°C (Fig. 4C). Aqueous liquid plus vapour inclusions from Nautanen range in salinity from 12 to 24 wt. % NaCl eq., with NaCl:$CaCl_2$ ratios typically ~1. Aqueous liquid plus carbonic liquid plus vapour inclusions at Nautanen and Aitik range in salinity from 4 to 21 wt. % NaCl eq. in the aqueous phase, with XCO_2 ranging from 0.02 to 0.29. Homogenisation to the liquid phase typically took place in the range 200-300°C. Carbonic liquid plus vapour

inclusions mostly showed T_mCO_2 from -56.6 to -59.0°C, with the majority of data between -56.6 and -57.0°C indicating a CO_2 dominated carbonic phase. These inclusions showed a wide range of densities, and homogenised to both the liquid and the vapour phase.

4.3 Crush leach and Laser Ablation ICP-MS analyses

The results of crush leach analyses are shown in Table 4, and representative LA-ICPMS analyses are shown in Table 5. The full data set for LA-ICPMS analyses is shown in the electronic Appendix. In all cases, the cationic composition of the brines is dominated by Na, Ca, K and Fe. In rare instances, the Fe concentration exceeded the K concentration. Concentrations of Mn, Sr, Ba, Zn, and Pb, are also significant, exceeding 1000 ppm in reconstructed fluid compositions in a number of cases. Copper concentrations are comparable in both data sets, ranging from tens to hundreds of ppm, and in rare case up to a few 1000, notably in individual fluid inclusion LA-ICPMS analyses compared to lower values in samples analysed by crush-leach methods. Boron and Li concentrations from the crush leach analyses are typically low, with Li below detection limits in some instances. Crush leach analyses also show significant sulphate concentrations in most fluids, ranging from ~10 to 5000ppm.

The results of crush leach and LA-ICPMS analyses are compared in Table 6. Analytical precision on leachate analyses is typically ~5%, whilst Allan et al. (2005) found accuracy typically around 15%, and precision was around 15%RSD for K, Rb and Cs, and 30% for other elements using LA-ICPMS. We have chosen to show a 30% error for all elements analysed by LA-ICPMS. Given that the crush-leach analyses represent a composition homogenised over many inclusions within a large

sample of quartz whilst the LA-ICPMS analyses are analyses of a limited number of individual inclusions the two data seta are reasonably consistent. For Fe oxide–apatite and IOCG-type fluids there is good agreement between crush-leach and LA-ICPMS analyses for individual samples for Na, Fe, K, Ca, Mn, Cu and B. There is greater spread in the LA-ICPMS data, as would be expected from the relatively low analytical precision, and from the analysis of individual inclusions, which trapped fluids during different stages of wall-rock interaction, precipitation and potentially mixing. However, significant differences do occur for K (in some samples), Ca (in some samples), Ba, B, and Br. Potassium values are only inconsistent for the sample from Kirunavaara where they are higher in the LA-ICPMS analyses than in the crush leach analyses. This may therefore represent sampling bias in the LA-ICPMS analyses. Although the microthermometric and LA-ICPMS data confirm that high Ca concentrations are characteristic of some fluids, the crush leach data gives some anomalously high Ca values. These may be related to contamination of the leachate by calcite on fracture surfaces. There is poor agreement between crush-leach analyses and LA-ICPMS data for Br. This is likely to be because Br only exceeded detection limits for LA-ICPMS in a limited number of the most saline and Br-rich inclusions. Bromine analysis of fluid inclusions by the methods used here has also been noted to give anomalously high Br concentrations from synthetic fluid inclusions (Allan et al., 2005), which Seo et al. (2011) attributed to remobilisation of Br from the ablation chamber and sample surface. As a result, Br/Cl ratios for inclusions analysed by LA-ICPMS are not included in the discussion and figures below.

5. Discussion

5.1 Trapping and ore formation conditions

For the vast majority of inclusions from the Fe oxide-apatite and IOCG deposits in this study there are a scarcity of relevant experimental data to constrain pressures at homogenisation and the positions of isochors. Very approximate estimates of P at T_h can be made from the data of Becker et al. (2008) by comparison of T_{sol}halite and T_hL-V with calculated isobars (Fig. 5A-C). Generally minimum trapping conditions for 'Fe oxide-apatite type' fluids are from 200-350°C and 200->300MPa, with those in chalcopyrite bearing veins from the Henry deposit potentially being even higher because of the presence of CO_2 (Schmidt and Bodnar, 2000), whilst those for 'IOCG type' fluids are from 300-450°C and 250 to >300MPa.

Early stages of fluid circulation at Aitik and Nautanen presumably took place under similar conditions to those seen in less deformed deposits (Wanhainen et al., 2005). The presence of secondary inclusion assemblages with complex mixtures of room temperature phase assemblage may provide better evidence for trapping conditions if they represent an unmixing assemblage (Fig. 5 D, E). Inclusions that homogenise by halite dissolution cannot represent part of an aqueous-carbonic fluid immiscibility assemblage, but mixed assemblages of Lw+Lc+V and Lc+V inclusions can, as can halite bearing inclusions which homogenise by vapour disappearance. For the sample studied at Aitik all Lw+Sh+V inclusions homogenise by halite dissolution, and so cannot have been formed by immiscibility. They hence indicate the presence of a fluid with salinities in the range 28-30 wt. % NaCl eq., comparable to fluids in veins cross-cutting the Fe oxide-apatite deposits. Aqueous-carbonic inclusions in trails with mixed Lw+Lc+V and Lc+V inclusions have estimated homogenisation pressures of 250-350MPa at temperatures of 200-290ºC, which provide minimum estimates of trapping conditions. Isochors for Lc+V inclusions which homogenise to a carbonic liquid do not intersect with those of the Lw+Lc+V inclusions and so either do not

represent part of an unmixing assemblage, or more likely given that these inclusion types occur on the same trails, contain a film of water which was not visible using transmitted light microscopy and hence may have homogenised at higher T and P than observed. The presence of Lc+V inclusions that homogenise to a carbonic vapour suggests pressures may have dropped even lower during periods of fracturing and vein dilation.

At Nautanen Lw+Sh+V inclusions homogenising by halite dissolution are also common, and so indicate similar saline fluids to those seen at Aitik. However, saline Lw+V inclusions, Lc+V, and Lw+Lc+V inclusions do co-exist, alongside some Lw+Sh+V inclusions which homogenise by vapour disappearance. Isochors for co-existing Lw+Lc+V, Lc+V, and Lw+V inclusions intersect (Fig. 5E), but do not have the same homogenisation temperature and pressures as would be required for definitive evidence of aqueous-carbonic fluid immiscibility (Ramboz et al., 1982). However, thin films of aqueous or carbonic fluids may be microthermometrically undetectable in the Lc+V and Lw+V inclusions respectively meaning that the trails with secondary populations are still consistent with immiscibility. The alternative, of mixing of aqueous and carbonic fluids cannot be ruled out, but would have been unlikely because of the difference in fluid density. In the case of immiscibility the homogenisation temperatures and pressures of the Lw+Lc+V inclusions indicate ranges ~240-370ºC and ~130-160MPa, and ~250-280 ºC and 25-55MPa. The wide range in homogenisation pressure is consistent with changes in fluid pressure during shear zone movement. The samples from the Ferrum Au prospect, peripheral to the main NDZ (Fig.5F), have a saline inclusion population with isochors similar to those from the saline populations from Aitik and Nautanen, but have no carbonic or aqueous-carbonic inclusions. The conditions of trapping of secondary calcic brine

inclusions in all deposits cannot be constrained beyond the plotting of representative isochors (Fig. 5F).

5.2 Source of salinity in the fluids.

Gleeson and Smith (2009) examined the potential sources of salinity in the sample set studied here using Br and Cl concentrations and chlorine stable isotope ratios. They concluded that whilst the Br/Cl ratios could be derived from either magmatic sources or halite dissolution, δ^{37}Cl values of Fe oxide-apatite and IOCG mineralisation-related quartz veins were lower than most crustal values and, hence, suggested magmatic input. However, some δ^{37}Cl values were very low and it was suggested that these may be the result of fractionation during extensive fluid-rock interaction between the fluids and Cl-rich phases (biotite and scapolite). The Br/Cl ratios and δ^{37}Cl values of vein fluids in NDZ-related deposits indicated a crustal origin for salinity and could indicate that the fluid salinity was sourced from either evaporites or from input from crustal melts, such as the granitic pegmatites of the Lina Suite that cut the Aitik deposit (Gleeson & Smith, 2009).

In this study, although a number of samples have Cl/Br ratios consistent with a magmatic source for the halogens, the Cl-enrichment apparent in the extended dataset (Fig. 6A),could be a strong indicator of interaction of fluids with (meta-) evaporites and consequent halite dissolution (Fig. 6B), followed by extensive water-rock interaction (Gleeson and Smith, 2009). No single group of inclusions or sample type shows a range of ratios consistent with a single fluid source, nor do high Cl/Br ratios correlate with the highest salinity fluids (Fig. 6C), which indicates that halite dissolution was not the only mechanism which generated highly saline brines. Typical magmatic-hydrothermal fluids are expected to have low salinities (Candela, 1989) and

salinities of ~6wt % NaCl eq. were used by Barton and Johnson (2000) for mass balance models of IOCG deposit formation. In this situation, however, highly saline magmatic brines could be produced by aqueous-carbonic fluid exsolution from magmas at relatively high pressure (compared with the porphyry environment) with subsequent separation and loss of water to a carbonic phase resulting in a high-salinity magmatic brine (Pollard, 2006). Brines associated with the NDZ show less evidence from Cl isotopes for fluid-rock interaction (Gleeson and Smith, 2009) and are significantly removed in time and tectonic setting from those involved in the formation of Fe oxide-apatite and IOCG mineralisation (Smith et al., 2009).

The complex range of sources for fluid components inferred above are consistent with the picture from IOCG type mineralisation globally, with deposits showing a complex mix of brine sources including magmatic-hydrothermal, evaporitic and surface fluids (e.g. Kendrick et al., 2007, 2008b) with some examples of deposits dominated by a single end-member (c.f. Williams et al., 2001). There remain issues with mixing models as the fluids involved frequently show high density contrasts, and there is abundant evidence for fluid overpressure in the form of hydraulic breccias in many districts, both of which would inhibit fluid mixing.

5.3 Controls on major element chemistry

The major element chemistry (Na, Ca, K, Fe and Mn) of crustal brines is controlled either by mineral-fluid equilibria, or, in cases where the buffer capacity of the host rock is exceeded, by the initial composition of the brine and the water-rock ratio (Yardley, 2005). It is rare in any of the deposits studied to see two feldspars in equilibrium, as albite replaces intermediate plagioclase in volcanic host rocks, and potassic alteration producing K-feldspar and biotite is common. Thus, the second of

the two cases above is more applicable to the alkali and alkaline earth metal concentrations in the hydrothermal systems. Most fluids are depleted in Na relative to the trend of halite dissolution by seawater. The Na-depletion is likely to relate to Na-Ca exchange reactions (albitisation and scapolitisation). The microthermometric data show that fluids in veins associated with Kiruna-type and IOCG mineralisation are strongly enriched in Na relative to Ca (Fig.7) and the LA-ICPMS and crush-leach data show that, except for in the late stage vein from Kiirunavaara, they are enriched in Na relative to K. The higher K content of the late Kiirunavaara brines suggests that the fluid trapped here is closer to a composition buffered by two feldspars, and potentially represents a less evolved fluid. In all these fluids K shows a strong positive correlation with Ba and Ba-rich K-feldspar has been reported from the IOCG deposit at Tjarrojakka (Edfelt et al., 2005).

At Gruvberget, and in both Aitik (Wanhainen et al., 2003) and Nautanen, strongly Ca-enriched fluids are found in secondary inclusions. The correlation of high Ca with high Na/K ratios (Fig. 7) is consistent with these fluids reacting with feldspar bearing assemblages at lower T than in the Fe oxide-apatite and IOCG related brines. High Ca contents can also be facilitated by low CO_2 fugacities, possibly following phase separation, resulting in a lack of buffering of Ca contents by calcite precipitation (Yardley, 2005). At Aitik, Wanhainen et al. (2003) attributed Ca-rich fluids to interaction of fluids with evaporites and anhydrite/gypsum dissolution. However, no concomitant increase in sulphate is seen, and there is little or no evidence of evaporitic sulphur in the region (Frietsch et al., 1995). The only other major source of Ca-rich fluids would be the dissolution of limestone. Intense magnetite and calc-silicate skarns do occur in the area (distinct from the magnetite-

apatite deposits) and hence limestone destruction may have acted as an additional source of Ca.

The fluids vary significantly in Fe content, in some cases to the extent that the brines are in fact Fe-dominant chloride solutions. This in part reflects the strong control of chlorinity on Fe solubility in most relatively reducing environments (Chou and Eugster, 1977; Kwak et al., 1986; Yardley, 2005). Iron was effectively mobilised from a volumetrically extensive zone during the regional albitisation and scapolitisation events that affected the Fennoscandian shield in northern Sweden and western Finland (Freitsch, 1997; Niiranen, 2005). Iron solubility is also controlled to a lesser degree by temperature and oxygen fugacity (Chou and Eugster, 1977;Yardley, 2005). The latter can be examined using the Fe/Mn ratio (Bottrell and Yardley, 1991), as Fe and Mn should exhibit contrasting redox behaviour. Unsurprisingly the Fe/Mn ratio correlates positively with the Fe content (Fig.8A). The data from the Nautanen prospect and Aitik deposits show lower Fe contents at a specific Fe/Mn ratio compared the Fe oxide-apatite deposits and IOCG-type deposits reflecting lower P-T conditions of trapping, and potentially different, Mn-depleted, host rocks. Copper concentrations show no correlation with the Fe-Mn ratio (Fig. 8B), suggesting a less significant redox control on copper solubility..

5.4 Metal transport and deposition

For a given source rock or magma the primary constraints on the metal bearing capacity of a hydrothermal solution are the availability of ligands, the temperature, the pH and the redox conditions (Barnes, 1979; Seward and Barnes, 1997; Wood and Samson, 1998; Yardley, 2005). In a significant proportion of natural solutions chloride is the predominant available anion for aqueous complex formation,

although HS^- maybe important for some metals (Seward and Barnes, 1997). Figure 9 shows plots of metal content against overall salinity. Within the relatively broad range of analytical values it is clear that salinity, and by inference chloride concentration, has a key effect on metal concentrations. Both pH and fO_2 are likely to have been strongly buffered by the alteration (feldspars and phyllosilicates) and oxide and sulphide mineral assemblages (magnetite-pyrite-hematite) in these deposits, and both are difficult to directly assess on the basis of fluid inclusion analyses alone. The effects of temperature are examined in Figure 10A-C, using fluid inclusion homogenisation temperatures (either halite dissolution or L-V homogenisation) as a proxy for trapping temperature. Correlations between T and metal concentration are poor for most metals with exception of Fe and Ag, which, despite the order of magnitude variations at any given T, show distinct high concentration clusters at high T (Fig. 10B). There may be some masking of the true trend here as the T_h values used are not corrected from pressure at trapping. Also the spread in data may be affected by the water-rock interaction history and the extent of equilibration with Fe-minerals. The effects of chlorinity can be normalised for by using the molal Me/Cl ratio (Yardley, 2005). Examples of these plots are shown in Figure 10F-H, which support interpretations of the influence of T on the solubility of Fe. For some transition metals (Cu and Pb) such a relationship is not apparent.

Cu contents in the hypersaline brines of the Pahtohavare deposit are typically in the range 100-500ppm, although some inclusions here and in the late stage Kiirunavaara veins have in excess of 1000ppm Cu. These ranges are comparable to saline magmatic fluids from the Cloncurry district, Australia (Baker et al., 2008), and are consistent with conclusions of Cu transport in saline brines in porphyry systems (Lerchbaumer and Audetat, 2012) The highest Cu contents are, however, in lower

salinity and temperature fluids from the NDZ. Previous work has identified solid sulphide inclusions on secondary trails in quartz from Aitik (Wanhainen et al., 2003), but these were not observed in the samples used in this study, and so we conclude that the data reflect real inclusion metal concentrations. A key control on elevated Cu concentrations may be high Cu contents in the source rocks and along the flow paths of the later hydrothermal fluids at Aitik and Nautanen, and, hence, a closer approach to saturation with Cu phases when compared to the earlier Fe oxide-apatite fluids (c.1890-1870Ma) and IOCG fluids (c. 1870-1860Ma). This interpretation is supported by Nd isotope data which indicate distinct sources for the two main mineralisation stages (Storey and Smith, in prep.). However, there is still a contrast between halite-bearing fluid inclusions and aqueous-carbonic brines at Nautanen and Aitik, which suggest other factors may also be important.

Diffusional loss or gain of Cu^{+} in fluid inclusions has been demonstrated experimentally (Li et al., 2009; Lerchbaumer and Audetat, 2012) via interdiffusion with Na^{+} and H^{+}, and to a lesser extent down concentration and electrochemical potential gradients. These studies involved Cu diffusion into very low salinity vapour inclusions, rather than the saline (10-20 wt. 5 NaCl eq.) aqueous-carbonic fluid observed here and so the conditions of the experiments did not reproduce those seen here. Analyses of some aqueous and aqueous carbonic fluid inclusions on single secondary trails show very consistent Cu contents (Appendix – NAU7706s) interpreted as trapping from a relative homogenous fluid in this case, and suggesting a lack of modification by post-entrapment diffusion. However, post-entrapment modification of inclusion Cu content cannot be entirely ruled out.

If high Cu contents in aqueous-carbonic fluids are not caused by post-entrapment modification, then the lack of correlation of high Cu with the most saline

brines suggests complexation of Cu by ligands other than Cl. Sulphur concentrations (as sulphate) are only available from crush-leach analyses in this study, but Figure 11 shows positive correlations between SO_4^{2-} and Cu concentration. Yardley et al. (1993) argued that crush-leach techniques are S-species specific, with H_2S escaping the gas phase during crushing. The oxygen fugacity and pH in ore mineral assemblages in these rocks are likely to have either been buffered by the assemblage pyrite plus magnetite, or in the NDZ-related deposits by assemblages including pyrrhotite. The positions of pyrite-magnetite boundary and the pyrite-pyrrhotite-magnetite triple point would in part also be controlled by the total sulphur content of the fluid (Bowman, 1998). For the lowest sulphate contents analysed here H_2S and HS^- would also be significant components of the fluid, whilst in the highest sulphate content fluids SO_4^- would predominate, but there would still be significant reduced S species. Hence, the order of magnitude variations in sulphate content of the leachate fluids may be taken as also indicate major variations in the concentration of the reduced sulphur species (Fig. 11). This suggests a role for complexation of metals by sulphur species, probably HS^-, in these fluids. High concentrations of sulphide species in low salinity fluids are consistent with the lower solubility of volatile species in aqueous solution with increasing salinity. Halite-bearing inclusions from both Aitik and Nautanen show lower Cu, Ag and Au concentrations than co-existing Lw+V and Lw+Lc+V inclusions. H_2S solubility in aqueous fluids decreases with increasing salt content with little temperature dependence except close to the critical point of water (Suleimanov and Krupp, 1994; Duan et al., 1996) in a similar way to CO_2. Data on CO_2-H_2S miscibility are lacking, but in most natural fluids H_2S concentrations are unlikely to be high enough to result in separation of two volatile-rich fluids and H_2S would remain completely miscible with a CO_2-rich aqueous carbonic phase. It is therefore

reasonable to suppose that bisulphide complexation will lead to elevated concentrations of metals acting as 'soft' Lewis acids (Cu, Au, Ag; Robb, 2005) in relatively low salinity, aqueous-carbonic solutions. The data presented here indicate that post-primary ore stage aqueous and aqueous-carbonic fluids in the NDZ hosted deposits, derived from either the local meta-volcanosedimentary rocks or from Lina stage crustal melts (Gleeson and Smith, 2009), transported significant Cu, Ag and possibly Au, resulting in grade increases as a result of addition of new metal, or by remobilisation of the primary ore. In mixed-volatile fluids, water activity coefficients rise above 1 at low pressures (~1.5kbar), but then fall with increasing temperature and pressure (Shmulovich and Graham, 1996). Aqueous-carbonic fluids may therefore be effective at forming outer sphere hydration shells (c.f. Williams-Jones and Heinrich, 2005) despite a lowered dielectric constant in the mixed solvent (Walther and Helgeson, 1980; Walther and Orville, 1983; Fein and Walther, 1987, 1989), at relatively shallow crustal depths, although there may be a preference for the occurrence of neutral complexes in solution.

The fact that mixed Lw+Sh+V, Lw+Lc+V and Lc+V inclusions exist on individual trails may be indicative of aqueous-carbonic fluid immiscibility. It has not been possible in this study to present full analyses of the CO_2-rich inclusions in these assemblages, as salinity could not be determined microthermometrically. Studies of vapour phase transport all emphasise the role of bisulphide complexation in the low density phase (e.g. Heinrich et al., 1999; Ulrich et al., 1999; 2001; Williams-Jones and Heinrich, 2005). It has now been demonstrated that S partitions strongly into the vapour phase on boiling in porphyry-type environments (Seo et al., 2009), and similar behaviour would be expected in aqueous-carbonic fluid immiscibility. However, at high XCO_2 outer sphere hydration shells implicated in vapour phase transport

(Williams-Jones and Heinrich, 2005) would breakdown, and so analogous behaviour of metals during aqueous-carbonic fluid immiscibility may not occur, and the preferentially partitioning of H_2S into the carbonic phase may actually be a trigger for metal deposition (Robb, 2005). The primary nature of high Cu contents in vapour inclusions has also now been called into question (Lerchbaumer and Audetat, 2012), suggesting immiscibility may be an effective trigger for Cu and possibly precious metal deposition. A full interpretation of these effects will require further analyses of CO_2-rich fluid inclusions.

6. Conclusions

The Fe oxide-apatite and IOCG deposits of the Kiruna and Malmberget districts, Sweden, formed from contrasting high salinity fluids at different times during the evolution of the districts. Deposits associated with major deformation zones show similar early fluid inclusions, but all have strongly overprinting fluid inclusion assemblages, with lower (but still highly saline) salinities, the presence of aqueous-carbonic fluids, and potentially immiscibility at some stages. These latter fluids are potentially related to a separate stage of hydrothermal circulation at ~1780Ma. Microthermometric constraints indicate minimum P-T conditions for Fe oxide apatite mineralisation of ~200-350°C and 200-300MPa and for IOCG mineralisation of ~300-450°C and 250 to >300MPa. Co-existing aqueous-carbonic, carbonic and saline fluid inclusions in deformed deposits associated with the NDZ indicate formation during a fluctuating pressure regime, potentially with periods of phase separation..

The Cl/Br ratios of inclusion fluids determined by crush-leach are consistent with a range of fluid sources including both magmas and halite-bearing evaporates.

The major element concentrations of the fluids are variable, and change between different stages of fluid circulation. Alkali metal concentrations appear to be unbuffered by rock mineral assemblages, consistent with the extensive alkali metasomatism in the area. Iron concentrations are strongly related to chlorinity, as are other metals such as Pb, consistent with chloride complexation control on solubility, with secondary controls from T and fO_2. Copper concentrations (and potentially Ag and Au) do not correlate with chlorinity in low salinity aqueous-carbonic fluids, and although post-entrapment modification of Cu concentrations cannot be ruled out, are inferred to be transported as bisulphide complexes in these lower salinity fluids. Low to moderate salinity and aqueous-carbonic fluids may have high H_2S concentrations, relative to highly saline fluids, and hence similar to higher metal carrying capacity.

Acknowledgements.

This work was originally funded by European Union Regional Development Fund Georange Program Grant 89121 to MS and SG. LA-ICPMS work was carried out at the NERC JIF sponsored facility at the University of Leeds, U.K. (NER/H/S/2000/853), with the assistance of L. Forbes and D. Banks. C. Storey assisted with field work in Sweden. The manuscript was improved by constructive comments from M. Barton and I. Samson.

Role of the funding source

The original field work and fluid inclusion work described in this manuscript were funded by European Union Regional Development Fund Georange Program Grant 89121. Apart from specifically funding work related to metallogeny and mineral exploration in Northern Sweden, this program played no role in the data collection or

interpretation beyond facilitating field work. The LA-ICPMS analyses were carried out at the UK Natural Environment Research Council sponsored facility (NERC Joint Infrastructure Fund) at the University of Leeds, U.K. (NER/H/S/2000/853). There is no influence from the funders on the data collection at this facility.

References.

Allan M.M.; Yardley, B.W.D.; Forbes, L.J., Shmulovich, K. I., Banks' D.A. and Shepherd' T.J. (2005).Validation of LA-ICP-MS fluid inclusion analysis with synthetic fluid inclusions. *Am. Mineral*., **90**, 1767-1775

Archer, D.G. (1992) Thermodynamic properties of the NaCl+H_2O system .2. thermodynamic properties of NaCl(aq), NaCl.2H_2O(cr), and phase-equilibria. *J. Phys.Chem. Ref. Data* **21,** 793-829

Baker T., Mustard R., Fu B., Williams P.J., Dong G., Fisher L., Mark G. and Ryan C.G. (2008) Mixed messages in iron oxide–copper–gold systems of the Cloncurry district, Australia: insights from PIXE analysis of halogens and copper in fluid inclusions. *Mineral. Dep.* **43**, 599-608.

Bakker R.J. (2003) Package FLUIDS 1. Computer programs for analysis of fluid inclusion data and for modelling bulk fluid properties. *Chem. Geol.* **194,** 3-23.

Barnes H.L. (1979) Solubilities of ore minerals. In *Geochemistry of hydrothermal ore deposits* (ed. H.L. Barnes). 2nd ed. Wiley, New York, p.404–459.

Barton M. D. and Johnson D. A. (1996) Evaporitic-source model for igneous-related Fe oxide-(REE–Cu–Au–U) mineralization. Geology 24, 259–262.

Barton M.D. and Johnson D.A. (2000) Alternative brine sources for Fe-oxide (-Cu-Au) systems: Implications for hydrothermal alteration and metals. In *Hydrothermal iron oxide copper-gold and related deposits: a global perspective*, (ed. T.M. Porter) Aus. Min. Found. Glenside, Australia, pp. 43-60.

Bastrakov, E.N., Skirrow, R.G., Davidson, G.J. (2007) Fluid evolution and origins of iron oxide Cu-Au prospects in the Olympic Dam district, Gawler Craton, South Australia. *Econ. Geol*. **102**, 1415-1440.

Becker S.P.; Fall A.; Bodnar R.J. (2008) Synthetic fluid inclusions. XVII. PVTX properties of high salinity H_2O-NaCl solutions (> 30 wt % NaCl): Application to fluid inclusions that homogenize by halite disappearance from porphyry copper and other hydrothermal ore deposits. *Econ. Geol*. **103**, 539-554.

Bergman S., Kübler L., and Martinsson O. (2001) *Description of the regional geological and geophysical maps of Northern Norrbotten County (east of the Caledonian orogen).* Geological Survey of Sweden (Sveriges Geologiska Undersökning). Ba56, 110p.

Bodnar R.J. (1993) Revised equation and table for determining the freezing-point depression of H2O-NaCl solutions. *Geochim. Cosmochim. Acta* **57**, 683-684.

Bodnar R.J. (1994) Synthetic fluid inclusions .12. The system H_2O-NaCl - experimental-determination of the halite liquidus and isochores for a 40 wt-percent NaCl solution. *Geochim. Cosmochim. Acta* **58**, 1053-1063.

Bottrell S.H., and Yardley B.W.D. (1991) The distribution of Fe and Mn between chlorite and fluid - evidence from fluid inclusions. *Geochim. Cosmochim. Acta* **55**, 241-244

Bowers T.S. and Helgeson H.C. (1983) Calculation of the thermodynamic and geochemical consequences of nonideal mixing in the system H_2O-CO_2-NaCl on phase relations in geologic systems: Equation of state for H_2O-CO_2-NaCI fluids at high pressures and temperatures**.** *Geochim. Cosmochim. Acta* **41**, 1247-1275.

Bowman J.R. (1998) Basic aspects and applications of phase equilibria in the Analysis of metasomatic Ca-Mg-Al-Fe-Si-S skarns. In: Lentz, D.R. (ed) *Mineralized intrusion-realted skarn systems*, Mineralogical Association of Canada Short course volume **26**, 99-145.

Boue-Bigne F.; Masters B.J.; Crighton J.S. and Sharp B. L. (1999) A calibration strategy for LA-ICP-MS analysis employing aqueous standards having modified absorption coefficients. *J. Anal. Atom. Spec*. **14**, 1665-1672.

Broman C. and Martinsson O. (2000) Fluid inclusions in epigenetic Fe-Cu-Au ores in Northern Norrbotten. In *2nd Annual GEODE Fennoscandian Shield workshop on Palaeo-proterozoic and Archaean greenstone belts and VMS districts in the Fennoscandian Shield: Gallivare-Kiruna. Sweden,* (eds. P.Weihed and O. Martinsson). Luleå Univeristy of Technology Research Report 2000,**6**, p7.

Candela P.A., (1989), Magmatic ore-forming fluids: Thermodynamic and mass transfer calculations of metal concentrations. *Rev. Econ. Geol*. 4, 203–221.

Carlon C.J. (2000) Iron oxide systems and base metal mineralisation in northern Sweden. In *Hydrothermal iron oxide copper-gold and related deposits: a global perspective,* (ed. T.M. Porter) Aust. Min. Found., Glenside, Australia pp. 283–296.

Chou I.M. and Eugster H.P. (1977) Solubility of magnetite in supercritical chloride solutions. *Am. J. Sci*. **277**, 1296-1314.

Diamond L.W. (1990) Stability of CO_2 clathrate hydrate+CO_2 liquid+CO_2 vapour+aqueous KCl-NaCl solutions - experimental-determination and application to salinity estimates of fluid inclusions. *Geochim. Cosmochim. Acta* **56**, 273-280.

Duan Z., Moller N., Weare J.H. (1996) Prediction of the solubility of H_2S in NaC1 aqueous solution: an equation of state approach. *Chem. Geol*. **130**, 15-20.

Edfelt A.,Armstrong R.N., Smith M., and Martinsson O. (2005) Alteration paragenesis and mineral chemistry of the Tjarrojakka apatite-iron and Cu (-Au) occurrences, Kiruna area, northern Sweden. *Mineral. Dep*. **40**, 409-434.

Ekdahl E. (1993) Early Proterozoic Karelian and Svecofennian formations and evolution of the Raahe-Ladoga ore zone, based on the Pielavesi area, central Finland. *Geol. Survey Finland Bull*. **373**, 1-137.

Fein J.B. and Walther J.V. (1987) Calcite solubility in supercritical CO_2-H_2O fluids. *Geochim. Cosmochim. Acta* **5**, 1665-1673.

Fein J.B. and Walther J.V. (1989) Portlandite solubilities in supercritical Ar-H_2O mixtures - implications for quantifying solvent effects. *Am. J. Sci.* **289**, 975-993.

Fontes J.C. and Matray J.M. (1993) Geochemistry and origin of formation brines from the Paris Basin, France .1. Brines associated with Triassic salts. *Chem. Geol.* **109**, 149-175.

Frietsch R., Tuisku P., Martinsson O. and Perdahl J.A. (1997). Early Proterozoic Cu-(Au) and Fe ore deposits associated with regional Na-Cl metasomatism in northern Fennoscandia. *Ore Geol. Revs*. **12**, 1-34.

Frietsch R., Billstrom K., and Perdahl J.A. (1995) Sulfur isotopes in lower Proterozoic iron and sulfide ores in northern Sweden. *Mineral. Dep*. **30**, 275-284.

Fu B., Williams P.J., Oliver N.H.S., Dong G.Y., Pollard P.J. and Mark G.M. (2003) Fluid mixing versus unmixing as an ore-forming process in the Cloncurry Fe-oxide-Cu-Au District, NW Queensland, Australia: evidence from fluid inclusions. *J. Geochem. Explor*. **78-9**, 617-622.

Geijer P. (1910) Igneous rocks and iron ores of Kiirunavaara,Luossavaara and Tuollavaara: scientific and practical researches in Lapland arranged by Luossavaara–Kiirunavaara Aktiebolag, Stockholm. p. 278.

Ghazi A.M. and Shuttleworth S. (2000) Trace element determination of single fluid inclusions by laser ablation ICP-MS: applications for halites from sedimentary basins. *Analyst* **125**, 205-210.

Gleeson S.A. and Smith M.P. (2009) The sources and evolution of mineralising fluids in iron oxide–copper–gold systems, Norrbotten, Sweden: Constraints from Br/Cl ratios and stable Cl isotopes of fluid inclusion leachates. *Geochim. Cosmochim. Acta* **73**, 5658–5672.

Gleeson S.A. and Turner W.A. (2007) Fluid inclusion constraints on the origin of the brines responsible for Pb-Zn mineralization at Pine Point and coarse non-saddle and saddle dolomite formation in southern Northwest Territories. *Geofluids* **7**, 51-68.

Groves D.I., Bierlein F.P., Meinert, L.D. and Hitzman M. (2010) Iron Oxide Copper-Gold (IOCG) Deposits through Earth History: Implications for Origin, Lithospheric Setting, and Distinction from Other Epigenetic Iron Oxide Deposits. *Econ. Geol.* **105**, 641-654.

Günther D., Frischknecht R., Muschenborn H.J., and Heinrich C.A. (1997) Direct liquid ablation: a new calibration strategy for laser ablation ICP-MS microanalysis of solids and liquids. *Fres. J. Anal. Chem.* **359**, 390-393.

Heinrich C.A., Günther D., Audétat A., Ulrich T., and Frischknecht R. (1999) Metal fractionation between magmatic brine and vapor, determined by microanalysis of fluid inclusions: *Geology*, **27**, 755–758.

Hitzman M.W., Oreskes N. and Einaudi M.T. (1992) Geological characteristics and tectonic setting of Proterozoic iron-oxide (Cu-U-Au-REE) deposits. *Precam. Res.* **58**, 241-287.

Hitzman M.W. (2000) Iron oxide-Cu-Au deposits: What, where, when and why In *Hydrothermal iron oxide copper-gold and related deposits: a global perspective*, (ed. T.M. Porter) Aus. Min. Found., Glenside, Australia p.9 -26.

Kendrick M.A., Baker T., Fu B., Phillips D., Williams P.J. (2008a) Noble gas and halogen constraints on regionally extensive mid-crustal Na–Ca metasomatism, the Proterozoic Eastern Mount Isa Block, Australia. *Precam. Res.* **163**, 131–150.

Kendrick M. A., Honda M., Gillen D., Baker T. and Phillips D. (2008b) New constraints on regional brecciation in the Wernecke Mountains, Canada from He, Ne, Ar, Kr, Xe, Cl, Br and I in fluid inclusions. *Chem. Geol*. **255**, 33–36.

Kendrick M.A., Mark G. and Phillips, D. (2007) Mid-crustal fluid mixing in a Proterozoic Fe oxide–Cu–Au deposit, Ernest Henry, Australia: Evidence from Ar, Kr, Xe, Cl, Br, and I. *Earth Planet. Sci. Letts* **256**, 328–343

Krumgalz B.S., Pogorelsky R., Pitzer K.S. (1996) Volumetric properties of single aqueous electrolytes from zero to saturation concentration at 298.15 K represented by Pitzer's ion-interaction equations. *J. Phys. Chem. Ref. Data* **25**, 639– 663.

Kwak T.A.P., Brown W.M., Abeysinghe P.B., Tan T.H. (1986) Fe solubilities in very saline hydrothermal fluids - their relation to zoning in some ore-deposits. *Econ. Geol.* **81,** 447-465.

Lerchbaumer, L. And Audetat, A. (2012) High Cu concentrations in vapor-type fluid inclusions: An artifact? *Geochim. Cosmochim. Acta* **88**, *255-274.*

Li Y., Audetat A., Lerchbaumer L., and Xiong X.L. (2009) Rapid Na, Cu exchange between synthetic fluid inclusions and external aqueous solutions: evidence from LA-ICP-MS analysis. *Geofluids* **9**, 321-329.

Lindblom S., Broman C. and Martinsson O. (1996) Magmatic-hydrothermal fluids in the Pahtohavare Cu–Au deposit in greenstone at Kiruna, Sweden. *Mineral. Dep.* **31,** 307–318.

Martinsson O. (2004) Geology and metallogeny of the Northern Norrbotten Fe-Cu-Au province. *Soc. Econ. Geol. Guidebook Series* **33**, 131-148.

Martinsson O. (1997). Tectonic Setting and Metallogeny of the Kiruna Greenstones. PhD Thesis, Luleå Univ. Tech.

Martinsson O. and Perdahl, J.-A. (1995) Paleoproterozoic extensional and compressional magmatism in northern Sweden. *In* J.-A. Perdahl: *Svecofennian volcanism in northern Sweden, Doctoral thesis 1995:169D, Paper II,* 1–13. Luleå University of Technology.

Martinsson O. and Virkkunen R. (2004) Apatite Iron Ores in the Gällivare, Svappavaara, and Jukkasjärvi Areas. *Soc. Econ. Geol. Guidebook Series* **33**, 167–172.

Martinsson O. and Wanhainen C. (2004) Character of Cu–Au mineralisation and related hydrothermal alteration along the Nautanen Deformation Zone, Gällivare Area, Northern Sweden. *Soc. Econ. Geol. Guidebook Series* **33,** 149–160.

Monro D. (1988) The geology and genesis of the Aitik Cu-Au deposit, arctic Sweden. Ph.D. Thesis, Department of Geology, Univ. Coll. Cardiff.

Niiranen T; Manttari I; Poutiainen M, Oliver N.H.S, and Miller J. (2005) Genesis of Palaeoproterozoic iron skarns in the Misi region, northern Finland. *Mineral. Dep*. **40,** 192-217.

Oakes C.S., Bodnar R.J. and Simonson J.M. (1990) The system NaCl-$CaCl_2$-H_2O .1. The ice liquidus at 1 atm total pressure. *Geochim. Cosmochim. Acta*, **54**, 603-610.

Pollard P.J. (2006) An intrusion-related origin for Cu-Au mineralization in iron oxide-copper-gold (IOGC) provinces. *Mineral. Dep*. **41**, 179-197.

Ramboz C., Pichavant M., and Weisbrod, A. (1982) Fluid immiscibility in natural processes – use and misuse of fluid inclusion data in terms of immscibility. *Chem. Geol.* **37**, 29-48.

Robb L. (2005) *Introduction to Ore-Forming Processes*. Blackwell Science.

Roedder E. (1984) Fluid inclusions. *Reviews in Mineralogy* **12**, Mineral. Soc. Amer.

Romer, R. L., Martinsson, O. & Perdahl, J.-A. (1994). Geochronology of the Kiruna iron ores and hydrothermal alteration. *Econ. Geol*. **89**, 1249^1261.

Seo J.H., Guillong M., and Heinrich C.A. (2009) The role of sulfur in the formation of magmatic–hydrothermal copper–gold deposits. *Earth Planet. Sci. Lett*. **282** 323–328.

Seo J.H., Guillong M., Aerts M., Zajacz Z., and Heinrich, C.A. (2011) Microanalysis of S, Cl, and Br in fluid inclusions by LA–ICP-MS. *Chem. Geol*. **284**, 35–44.

Seward T.M., and Barnes H.L. (1997) Metal transport by hydrothermal ore fluids. In *Geochemistry of hydrothermal ore deposits* (ed. H.L. Barnes) 3rd ed., Wiley, New York, 435–486.

Schmidt C. and Bodnar R.J. (2000) Synthetic fluid inclusions: XVI. PVTX properties in the system H_2O-NaCl-CO_2 at elevated temperatures, pressures and salinities. *Geochim. Cosmochim. Acta* **64**, 3853-3869.

Shmulovich K.I., and Graham C.M. (1996) Melting of albite and dehydration of brucite in H_2O-NaCl fluids to 9 kbars and 700-900 degrees C: Implications for partial melting and water activities during high pressure metamorphism. *Contrib. Mineral. Pet.* **124**, 370-382.

Skiöld T. (1987) Aspects of the Proterozoic Geochronology of northern Sweden. *Precam. Res.* **35,** 161–167.

Smith M. P., Storey C. D., Jeffries T. E. and Ryan C. (2009) In-situ U-Pb and trace element analysis of accessory minerals in the Kiruna district, Norrbotten, Sweden: new constraints on the timing and origin of mineralisation. *J. Petrol*. **50**, 2063-2094.

Span R and Wagner W. (1996) A new equation of state for carbon dioxide covering the fluid region from the triple-point temperature to 1100 K at pressures up to 800 MPa. *J. Phys. Chem. Ref. Data* **25**, 1509-1596

Sterner S. M., Hall D. L. and Bodnar R. J. (1988) Synthetic fluid inclusions. V. Solubility relations in the system NaCl–KCl–H_2O under vapour-saturated conditions. *Geochim. Cosmochim. Acta* **52**, 989–1005.

Storey C. D., Smith M. P. and Jeffries T. E. (2007) In situ LA-ICPMS U–Pb dating of metavolcanics of Norrbotten, Sweden: records of extended geological histories in complex titanite grains. *Chem. Geol.* **240**, 163–181.

Suleimenov M. and Krupp R.E. (1994) Solubility of hydrogen sulfide in pure water and in NaCl solutions, from 20 to 320°C and at saturation pressures. *Geochim. Cosmochim. Acta* **58**, 2433-2444.

Ulrich T., Günther D., and Heinrich C.A. (1999) Gold concentrations of magmatic brines and the metal budget of porphyry copper deposits. *Nature*, **399**, 676–679.

Ulrich T., Günther D., and Heinrich C.A. (2001) Evolution of a porphyry Cu-Au deposit, based on LA-ICP-MS analysis of fluid inclusions, Bajo de la Alumbrera, Argentina. *Econ. Geol*. **96**, 1743 –1774.

Walther J.V. and Helgeson H.C. (1980) Description and interpretation of metasomatic phase-relations at high-pressures and temperatures .1. Equilibrium activities of ionic species in nonideal mixtures of CO_2 and H_2O. *Am. J. of Sci.* **280**, 575-606.

Walther J.V and Orville P.M.(1983) the extraction quench technique for determination of the thermodynamic properties of solute complexes - application to quartz solubility in fluid mixtures. *Am. Mineral*. **68**, 731-741.

Wanhainen C., Billstrom K., Martinsson O., Stein H. and Nordin R. (2005) 160 Ma of magmatic/hydrothermal and metamorphic activity in the Gallivare area: Re-Os dating of molybdenite and U-Pb dating of titanite from the Aitik Cu-Au-Ag deposit, northern Sweden. *Mineral. Dep.* **40**, 435-447.

Wanhainen C., Broman C. and Martinsson O. (2003) The Aitik Cu-Au-Ag deposit in northern Sweden: a product of high salinity fluids. *Mineral. Dep.* **38**, 715-726.

Williams P.J., Barton M.D., Johnson D.A., Fontbote L., de Haller A., Mark G., Oliver N.H.S., and Marschik R. (2005) Iron oxide copper gold deposits; geology, space–time distribution, and possible modes of origin. *Econ. Geol.* **100**, 371–405.

Williams P.J., Dong G.Y., Ryan C.G., Pollard P.J., Rotherham J.F., Mernagh T.P. and Chapman L.H. (2001) Geochemistry of hypersaline fluid inclusions from the Starra (Fe oxide)-Au-Cu deposit, Cloncurry district, Queensland. *Econ. Geol*. **96**, 875-883.

Williams-Jones A.E. and Samson I.H. (1990) Theoretical estmation of halite solubility in the ystem NaCl-CaCl2-H2O: Applications to fluid inclusions. *Can. Mineral.* **28**, 299-304.

Williams-Jones A.E. and Heinrich C.A. (2005) Vapor Transport of Metals and the Formation of Magmatic-Hydrothermal Ore Deposits. *Econ. Geol*. **100**, 1287-1312.

Wood S.A., and Samson I. (1998) Solubility of ore minerals and complexation

of ore metals in hydrothermal solutions. *Rev. Econ. Geol.* **10**, 33–80.

Yardley B.W.D. (2005) Metal Concentrations in Crustal Fluids and Their Relationship to Ore Formation. *Econ. Geol*. **100**, 613-632.

Yardley, B.W.D., Banks, D.A., and Bottrell, S.H. (1993) Post-metamorphic gold-quart veins from N.W. Italy: the composition and origin of the ore fluid. *Mineral. Mag*. **57**, 407-422.

Zhang Y.G. and Frantz J.D. (1987) Determination of the homogenization temperatures and densities of supercritical fluids in the system NaCl-KCl-$CaCl_2$-H_2O using synthetic fluid inclusions. *Chem. Geol.* **64**, 335-350.

Tables

Table 1: Localities and descriptions of samples used in this study. Northings and eastings are given in Swedish National Grid Co-ordinates (RTG80).

Table 2: Summary of fluid inclusion petrography and the results of microthermometric measurements. All measurements in ºC.

Table 3: Summary of fluid inclusion compositions determined from microthermometry.

Table 4: Representative results of analyses of fluid inclusion leachates from vein quartz. Fluid compositions were reconstructed by charge balance of total cations against Cl molality determined from microthermometric data (Allen et al., 2005). All concentrations reported in ppm.

Table 5: Table 5: Representative examples of LA-ICPMS analyses of fluid inclusions. Compositions are shown in ppm as either total cations charge balanced against Cl molality from microthermometry (Allen et al., 2005) or normalised to Cl concentration in ppm where the major cations had not been analysed.Table 6: Comparison of reconstructed fluid composition from crush-leach analyses

with mean reconstructed fluid inclusion composition from LA-ICPMS analyses. All concentrations in ppm.

Electronic Appendix: Results of microthermometry and LA-ICPMS analyses of fluid inclusions, reconstructed from microthermometrically determined salinity using the method of Allan et al., (2005).

Figures

Figure 1: Geological sketch map of northern Norrbotten county, showing the locality of the deposits and prospects used in this study. Geology adapted from Bergman et al. (2001).

Figure 2: Meso- to microscale textures in quartz veins from the studied deposits. (a) Quartz-actinolite vein cutting magnetite-albite altered wall rocks, Nuktus. (b) Plane polarised, transmitted light photomicrograph of quartz-carbonate vein cutting magnetite ore, Luossavaara. The vein hosts titanite, now partly altered to rutile (sample L4.1). The highlighted area is magnified in (c). (c) Plane polarised, reflected light photograph of area highlighted in (a). There is no visible alteration of magnetite in the vein wall rock. (d) Quartz-chalcopyrite-ankerite vein cutting magnetite-albite altered metavolcanic rock, Pahtohavare. (e) Plane polarised, reflected light photograph of quartz-magnetite-sulphide vein, Pahtohavare (P11). (d) Plane polarised, combined reflected and trasnmitted light photograph of quartz-sulphide vein sample A3, Aitik. Sulphide minerals below the surface of the sample in fractures in quartz are visible as opaque areas. Act – Actinolite; Alb – Albite; Ank – Ankerite; Cpy –

Chalcopyrite; Prt – Pyrrhotite; Py – Pyrite; Qtz – Quartz; Mgt – Magnetite; Rt – Rutile; Ttn – titanite.

Figure 3: Petrography of fluid inclusions in studied quartz vein samples. (a) Fragment of polished wafer from N2.2 showing fluid inclusions along face parallel trails and growth zones in quartz. See Gleeson and Smith (2009) for further evidence for primary fluid inclusion origin. (b) Lw+Sh+V inclusion in quartz, Nuktus. (c) Lw+Sh+Lc+V inclusions in quartz, Henry. (d) Lw+nS+V inclusions in quartz, Pahtohavare. (e) Lw+nS+V inclusions in quartz, Gruvberget. (f) Lw+Sh+V inclusion in quartz, Nautanen. (g) Lc+V inclusions in quartz, Nautanen. (h) Lw+Sh+V in clear secondary trail, Aitik. (i) Single secondary fluid inclusion trail bearing Lc+V and Lw+Lc+V inclusions, Nautanen.

Figure 4: Results of fluid inclusion microthermometry in terms of T_hL-V and total salinity as wt. % NaCl eq, and NaCl-$CaCl_2$ ratio from samples from (a) Fe oxide-apatite deposits.; (b) IOCG deposits; and (c) Deformed deposits associated with the NDZ.

Figure 5: Estimates of P and T at homogenisation and trapping for different deposit types. (a)-(c) Comparison of microthermometric data from this study with isobars of P (in MPa) at halite dissolution from Becker et al. (2008). In nearly all cases studied here the homogenisation conditions are outside the calibrated range. (d) Isochors for different fluid inclusion populations from Aitik sample A3. (e) Representative isochors for fluid inclusions from the Nautanen Cu-Au

prospect. A – approximate range of P at Th for fluid inclusion homogenising by halite dissolution. B – Zone of P at T_h for the Lw+Lc+V inclusions occupying secondary trails with Lc+V inclusions. These may indicate trapping conditions for an immiscibility assemblage, and the conditions of at least one stage of ore genesis. Termination of isochores for Lw+Lc+V inclusions indicates P at T_h. (f) Approximate range of P at Th, and representative isochores for fluid inclusions from the Ferrum deposit. See text for details of isochore location and phase boundary construction.

Figure 6: Halogen geochemistry of fluid inclusions from the Norrbotten district. (a) Comparison of Cl and Br concentrations in reconstructed inclusion fluids with the seawater evolution trends from Fontes and Matray (1993). (b) Molal Na/Br and Cl/Br ratios compared with the ranges of ratios from seawater and 'magmatic' fluids, and the halite dissolution trend. (c) Plot of molal Cl/Br ratio against fluid inclusion salinity determined from microthermometry.

Figure 7: Ternary plots of fluid inclusion major element chemistry (as mass %) from crush leach and LA-ICPMS analyses. The shaded areas in each plot show the range of Na:Ca ratios determined from microthermometry.

Figure 8: Plots of reconstructed Cu and Fe concentrations against Fe/Mn ratio of fluid inclusion leachates and LA-ICPMS analyses.

Figure 9: Plots of reconstructed transition and precious metal concentration against salinity as determined from microthermometry.

Figure 10: (a)-(e) Plots of metal concentration against fluid inclusion homogenisation temperature. (f)-(h) Representative plots of molal metal/chloride ratio against 1/T. The normalisation of metal to chloride removes the effects of salinity on concentration, and allows the effects of T to be more fully assessed.

Figure 11: Variation in key metal concentrations with sulphate content of fluid inclusion leachates. Sulphur was not analysed by LA-ICPMS in this study.

Sample No	Site Name	Northing	Easting	Depth	Description
Magnetite-(Hematite)-apatite bodies.					
KR2	Kiirunavaara	7534661	1684696	Surface	Quartz-actinolite-hematite vein in hanging wall metavolcanic breccia.
L4.1	Luossavaara	7538046	1685661	Surface	Aplitic quartz-carbonate vein cutting magnetite ore.
HEN04	Henry	7539907	1686986	Surface	Quartz-chalcopyrite vein cutting magnetite ore.
N1	Nuktus	7538978	1686396	Surface	Quartz-hematite vein cutting chloritic schist.
N2.2	Nuktus	7540615	1687048	Surface	Quartz-hematite-ankerite vein cutting hematite ore.
N2.5	Nuktus	7540615	1687048	Surface	Quartz-amphibole vein cutting partially altered rock.
MER2	Mertainen	7520872	1710539	Surface	Quartz-albite-tourmaline vein cutting magnetite ore.
Greenstone- and Porphyry- hosted Cu mineralisation					
KALL91002	Kallosalmi	7541825	1693135	59.53m	Quartz vein cutting biotite-scapolite-graphite schist
PAH88217	Pahtohavare	7527612	1680390	21.20m	Quartz vein cutting biotite-scapolite schist.
PAH85117	Pahtohavare	7527159	1680702	152.14m	Quartz-carbonate vein in biotite-scapolite schist.
P11	Pahtohavare	7527555	1680370	Surface	Quartz-chalcopyrite-bornite vein.
K2	Kiskamavaara	7534093	1725127	Surface	Quartz vein in hematite cemented K-altered metavolcanic breccia.
G6	Gruvberget	7515227	1719947	Surface	Quartz vein from Stokenstrom mine spoil.
G5.1	Gruvberget	7515149	1719979	Surface	Quartz vein with malachite cutting K-altered metavolcanics.
GRUV02	Gruvberget	7515134	1719951	Surface	Quartz vein at sheared margin of ore body.
GRUV06	Gruvberget	7515255	1719961	Surface	Quartz vein cutting magnetite ore body.
Nautanen Deformation Zone(NDZ)-hosted Cu mineralisation					
NAU 77006	Nautanen	7463947	1719762	210.47m	Quartz-chalcopyrite vein cutting biotite-actinolite schist.
NAU 77006	Nautanen	7463947	1719762	281.7m	Quartz-chalcopyrite vein cutting biotite-actinolite schist.
NAU02	Nautanen	7463815	1719453	Surface	Folded quartz vein in psammitic garnet schist.
NAU83009	Nautanen	7463843	1719634	110.90m	Quartz-chalcopyrite vein cutting biotite schist.
NAU05	Nautanen	7463626	1719521	Surface	Quartz vein cutting bornite mineralised bt-qtz-ep schist.
NAU09	Nautanen	7461151	1719406	Surface	Foliation parallel quartz vein in biotite-magnetite schist.
FERR69205	Ferrum	7463076	1722146	72.75m	Quartz vein cutting K-feldspar-epidote-actinolite altered schist.
FERR69203	Ferrum	7463080	1722150	54.58m	Quartz vein with sulphides.
FERR69202	Ferrum	7463110	1722160	6.43m	Quartz vein with malachite and bornite
A3	Aitik	7545020	1724300	Surface	Quartz-chalcopyrite vein - main ore zone

Table 1: Localities and descriptions of samples used in this study. Northings and eastings are given in Swedish National Grid Co-ordinates (RTG80).

	N	Inclusion Type		T_{fm} Range	T_m CO_2	T_m hh	T_m ice	T_m Clathrate	T_h CO_2	T_h L-V	T_{sol} Halite
Magnetite-(Hematite)-apatite bodies.											
KR2	28	Lw+Sh+V	P/PS/S	-48 to -55		6	-35			102	224
L4.1	28	Lw+Sh+V	P/PS/S	-52 to -62		10	-29			122	278
HEN04	16	Lw+Sh(+Lc)+V	P/PS/S	-44 to -68	-56.9	5	-27		24.9	118	249
	10	Lw+Lc+V	PS/S	-28 to -51	-57.1		-26.6	-11.2	21.6	212	
N1	28	Lw+Sh+V	P/PS/S	-52 to -67		12	-30			150	225
N2.2	24	Lw+Sh+V	P/PS/S	-58 to -69		12	-28.8			103	252
N2.5	21	Lw+Sh+V	P/PS/S	-57 to -66		10	-27.8			110	258
MER2	25	Lw+nS+V	PS/S	-60 to -70		14	-27.3			145	437
	8	Lw+Sh+V	S	-32 to -62		12.8	-24.5			106	108
Greenstone- and Porphyry- hosted Cu mineralisation											
KALL91002	15	Lw+nS+V	P/PS	ND						139	404
	11	Lw+Sh+V	PS/S	-66 to -72						101	207
	6	Lw+V	PS/S	-51 to -53			-22.3			120	ND
PAH88217	16	Lw+nS+V	P/PS/S	ND						119	452
PAH85117	19	Lw+nS+V	P/PS/S	-44 to -59			-15.1			161	412
		Lc+V	PS/S		-59.7				-6.2		
P11	23	Lw+nS+V	P/PS/S	-54 to -63		11	-25.8			137	375
K2	27	Lw+Sh+V	P/PS/S	-58 to -70		15	-25.9			118	229
G6	22	Lw+nS+V	P/PS	-45 to -65		12	-26.9			119	352
	8	Lw+Sh+V	PS/S							128	336
G5.1	16	Lw+nS+V	P/PS							130	246
	21	Lc+V	PS/S		-57.1				8.6		
GRUV02	14	Lw+Sh+V	PS/S							105	185
	21	Lw+V	PS/S	-53 to -72		-34.5	-13.3		-8.7	137	
	15	Lc+V	S		-56.6						
GRUV06	28	Lw+V	PS/S	-56 to -70		-43.9	-36.5			98.2	
Nautanen Deformation Zone(NDZ)-hosted Cu mineralisation											
NAU 77006	13	Lw+Lc+V	PS/S	-40 to -59	-56.8			0.2	28.1	263	
	40	Lw+Sh+V	PS/S	-52 to -65		6.1	-23.7			196	247
	48	Lw+V	PS/S	-43 to -72		-27.9	-15.2			155	
	15	Lc+V	PS/S		-56.7				6.3		
NAU 77006	29	Lw+Sh+V	PS/S	-52 to -66		1.6	-26.3			138	188
	20	Lc+V	PS/S		-56.6				2.6		
03NAU02	7	Lw+Sh+V	PS/S							154	199
	7	Lc+V	PS/S		-56.6				-8.4		
NAU83009	30	Lw+Sh+V	PS/S	-63 to -73						145	158
	3	Lw+Lc+V	PS/S		-56.6			4	29.3	269	
	7	Lc+V	PS/S		-56.7				28.5		
NAU05	26	Lw+Sh+V	PS/S	-52 to -57		-18.3	-27			173	345
	26	Lw+V	PS/S	-72 to -76		-41.4	-27.6			136	
	9	Lc+V	PS/S		-56.7				-6.8		
NAU09	26	Lw+Sh+V	PS/S	-53 to -70		-10.9	-34.3			162	231
	12	Lw+V	PS/S	-52 to -58		-29.9	-22.8			132	
A3	34	Lw+Sh+V	PS/S	-79 to -64		12.6	-28.3			111	131
	39	Lw+Lc+V	S	-65 to -45	-57.4			-1.3	17.6	243	
	11	Lw+V	S	-62 to -58						104	
	16	Lc+V	S		-57.8				2.7		
FERR69205	3	Lw+Sh+V	PS/S							141	180
	18	Lw+V	PS/S	-52 to -69		-36.6	-18.7			152	
FERR69203	13	Lw+Sh+V	PS/S	-59 to -63		1	-28.8			156	212
	16	Lw+V	PS/S	-64 to -72		-35.3	-24.7			135	
FERR69202	27	Lw+V	S	-66 to -73		-35.1	-18.9			154	
	7	Lw+V	S	-48 to -51			-0.6			160	

1) P - Primary; PS - Pseudosecondary; S - Secondary

Table 2: Summary of fluid inclusion petrography and the results of microthermometric measurements. All measurements in ºC.

	N	Inclusion types[1]		XCO_2		Salinity (wt. % NaCl eq.)[2]		Salinity (wt. % $NaCl+CaCl_2$)[3]		Na:Ca by mass
				mean	range	mean	range	mean	range	mean
Magnetite-(Hematite)-apatite bodies.										
KR2	28	Lw+Sh+V	P/PS/S	ND		33.2	31.4-36.6			
L4.1	28	Lw+Sh+V	P/PS/S	ND		36.5	33.4-41.2	41	36-46	4.1
HEN04	16	Lw+Sh(+Lc)+V	P/PS/S	0.02	0.01-0.03	34.7	33.3-37.9			
	10	Lw+Lc+V	PS/S	0.04	0.03-0.06	21.4	21.4-21.5			
N1	28	Lw+Sh+V	P/PS/S	ND		33.3	31.5-35.3	37	34-38	2.4
N2.2	24	Lw+Sh+V	P/PS/S	ND		34.9	32.9-39.4	38	34-43	3.4
N2.5	21	Lw+Sh+V	P/PS/S	ND		35.3	31.5-38.5	38	34-43	3.7
MER2	25	Lw+nS+V	PS/S	ND		52.0	40.2-59.5	56	55-58	16.2
Greenstone- and Porphyry- hosted Cu mineralisation										
KALL91002	15	Lw+nS+V	P/PS	ND		49.1	32.7-61.1	50	38-55	5.2
	11	Lw+Sh+V	PS/S	ND		32.2	31.6-32.9			
	6	Lw+V	PS/S	ND		24.2	23.9-24.8			
PAH88217	16	Lw+nS+V	P/PS/S	ND		53.6	46.3-57.4			
PAH85117	19	Lw+nS+V	P/PS/S	ND		49.0	41.4-57.0			
		Lc+V	PS/S	Lc+V inclusions						
P11	23	Lw+nS+V	P/PS/S	ND		42.0	34.1-49.1	48	44-51	14.7
K2	27	Lw+Sh+V	P/PS/S	ND		33.5	31.1-37.2	35	34-36	4.9
G6	22	Lw+nS+V	P/PS	ND		42.8	38.1-48.8	45	41-52	7.3
	8	Lw+Sh+V	PS/S	ND		41.1	40.5-41.6			
G5.1	16	Lw+nS+V	P/PS	ND		34.5	33.2-37.1			
		Lc+V	PS/S	Lc+V inclusions						
GRUV02	14	Lw+Sh+V	PS/S	ND		31.3	28.9-33.3			
	21	Lw+V	PS/S	ND		16.8	10.2-23.6	16	12-22	0.4
		Lc+V	S	Lc+V inclusions						
GRUV06	28	Lw+V	PS/S	ND		33.1	27.1-41.2	28	24-33	0.27
Nautanen Deformation Zone(NDZ)-hosted Cu mineralisation										
NAU 77006	5	Lw+Lc+V	PS/S	0.18	0.17-0.20	9.1	3.7-12.4			
	17	Lw+Sh+V	PS/S	ND		34.8	31.5-41.0	36	32-43	12.3
	22	Lw+V	PS/S	ND		19.4	12-28.3	18.6	23-23	2.4
		Lc+V	PS/S	Lc+V inclusions						
NAU 77006	18	Lw+Sh+V	PS/S	ND		33.2	31.3-35.0			
	11	Lw+Sh+V	PS/S	ND		28.9	27.8-29.9			
		Lc+V	PS/S	Lc+V inclusions						
03NAU02	20	Lw+Sh+V	PS/S	ND		33.2	30.2-35.4			
		Lc+V	PS/S	Lc+V inclusions						
NAU83009	30	Lw+Sh+V	PS/S	ND		29.3	26.2-32.3			
	3	Lw+Lc+V	PS/S	0.23	0.19-0.29	10.3	6.7-12.9			
		Lc+V	PS/S	Lc+V inclusions						
NAU05	26	Lw+Sh+V	PS/S	ND		43.5	31-51.8			
	26	Lw+V	PS/S	ND		27.7	21.9-32.5	25.2	22-26	0.4
	9	Lc+V	PS/S	Lc+V inclusions						
NAU09	26	Lw+Sh+V	PS/S	ND		33.6	32-36.5	38.7	37-42	2.5
	12	Lw+V	PS/S	ND		24.5	21.9-26.5			
A3	34	Lw+Sh+V	PS/S	ND		29.0	28.2-29.6			
	39	Lw+Lc+V	S	0.1	0.05-0.29	16.0	9.7-21.1			
	11	Lw+V	S	ND		15.7	15.4-15.9			
	16	Lc+V	S	Lc+V inclusions						
FERR69205	3	Lw+Sh+V	PS/S	ND		31.3	28.1-33.9			
	18	Lw+V	PS/S	ND		21.7	18.6-24.0			
FERR69203	13	Lw+Sh+V	PS/S	ND		32.8	29.1-35.9	35.1	34-38	2.7
	16	Lw+V	PS/S	ND		25.8	24.1-27.2	23.7	22-25	0.3
FERR69202	27	Lw+V	S	ND		21.8	19.7-25.4	19.8	19-23	0.3
	7	Lw+V	S	ND		1.0				

1) P - Primary; PS - Pseudosecondary; S - Secondary
2) Sterner et al. (1988)
3) Oakes et al. (1990)

Table 3: Summary of fluid inclusion compositions determined from microthermometry.

Sample	Detection limits (ppm)	Kiruna Fe-apatite				Kiruna Cu				Gruvberget Fe-oxide Cu			NDZ				
		N2.5	L4.1	KR2	HEN04	PAH 88217	K2	PAH01	KALL 91002	G6	G5.1	GRUV06	NAU09	NAU05	NAU 83009	NAU 77006	FERR 69203
Salinity (wt. % NaCl eq.)		35.3	36.5	33.2	34.7	53.6	33.5	54.3	49.1	42.8	34.5	28.0	33.6	43.5	29.9	28.0	28.9
2σ		3.4	6.0	2.2	3.3	6.1	2.8	5.6	18.0	7.3	2.1	4.0	2.2	16.3	2.5	17.1	8.6
Cl	0.002	13.5	8.1	16.0	87.3	19.1	39.9	114.5	32.9	21.4	19.0	28.2	21.9	7.6	12.3	32.7	31.8
Br	0.001	0.022	0.022	0.018	0.062	BD	0.021	0.120	0.020	0.010	0.015	0.029	0.027	BD	BD	0.046	0.038
Sulfate	0.001	0.101	0.110	0.093	1.740	0.001	0.649	0.860	BD	0.050	0.066	1.226	0.140	0.597	BD	BD	0.002
Na	0.002	8.1	11.1	7.2	32.2	11.1	22.9	46.4	12.6	12.6	10.2	15.9	9.2	4.1	5.1	13.0	5.8
K	0.002	2.1	2.9	1.8	5.7			2.3	2.1			1.5	1.3	0.2	1.4	3.2	1.7
Li	0.002	0.016	0.012	0.016	0.062				BD				0.026	0.006	0.010	0.004	0.007
Ca	0.2	3.6	7.1	5.3	13.5	3.1	5.2	41.6	10.5	4.1	8.5	16.0	7.0	2.8	3.5	4.3	5.9
Fe	0.01	0.36	0.57	0.10	1.41	1.18	4.99	9.05	2.55	1.54	0.41	1.69	0.30	1.46	0.24	0.98	0.28
Mn	0.005	0.20	0.77	0.45	0.52	0.38	1.17	1.93	0.55	0.98	0.47	0.92	0.26	0.30	0.19	0.33	0.07
Pb	0.0001	0.07	0.07	0.07	0.14	0.02	0.09	0.09	2.11	0.09	0.78	0.04	0.02	0.02	0.06	0.01	0.01
Zn	0.001	0.14	0.28	0.27	0.24	0.08	0.25	0.35	0.10	0.13	0.08	0.09	0.14	0.21	0.07	0.13	0.05
Sr	0.001	0.14	0.20	0.27	0.33	0.07	0.32	0.46	0.10	0.10	0.14	0.18	0.08	0.05	0.06	0.09	0.12
Ba	0.001	0.70	0.72	0.85	0.60	0.22	6.28	2.61	0.25	0.17	0.17	0.34	0.07	0.35	0.07	0.14	0.05
Al	0.05	0.015	0.055	0.035	0.052	0.082	0.176	0.138	0.081	0.151	0.315	0.099	0.061	0.092	0.073	0.348	0.124
Cu	0.0001	0.006	0.013	0.011	0.031	0.006	0.072	0.069	0.012	0.504	0.616	0.157	0.014	0.172	0.009	0.067	0.028
B	0.002	0.012	0.040	0.046	0.102	0.006	0.069	0.038	0.048	0.138	0.071	0.029	0.041	0.028	0.075	0.041	0.080
Co	0.0001	0.001	0.001	0.0007	0.001	0.0008	0.005	0.003		0.005	0.002	0.002					
As	0.0002	0.005	0.005	0.001	0.018	0.001	0.022	0.010	0.003	0.013			0.008	0.003	0.011	0.004	0.003
Cd	0.00001	0.001	0.001	0.001	0.001	0.0004	0.0005	0.001		0.0005	0.0002	0.0005	0.001	0.0004	0.0001	0.001	0.0001
Reconstructed fluid composition																	
Na		120353	100834	92202	131548	227301	110470	148134	125582	12846	78279	70638	90549	87822	67340	91126	60997
K		31150	26535	23051	23424	0	0	7351	20684	0	0	6789	13203	4498	18067	22091	17537
Li		241	106	204	252	0	0	0		0	0	0	257	125	132	28	76
Ca		53805	64746	67835	55057	63228	25288	132858	104898	42044	65232	71181	69421	59145	46365	30375	61759
Fe		5380	5201	1317	5758	24171	24090	28932	25486	15650	3131	7498	2943	31186	3091	6825	2897
Mn		3058	7027	5809	2122	7779	5670	6157	5466	9951	3653	4097	2611	6452	2539	2308	686
Pb		1076	653	909	576	422	431	282	21127	911	6027	178	192	446	729	64	95
Zn		2039	2516	3497	967	1729	1224	1130	960	1331	626	386	1336	4534	971	935	564
Sr		2138	1794	3444	1332	1377	1531	1458	953	1051	1096	820	792	1129	828	655	1266
Ba		10407	6549	10867	2438	4466	30346	8356	2453	1728	1331	1511	649	7599	905	1002	557
Al		227	499	448	214	1681	852	440	813	1542	2427	440	596	1972	960	2434	1296
Cu		92	117	145	126	128	346	220	118	5139	4749	696	136	3674	121	465	297
B		177	361	586	416	128	333	120	480	1401	548	130	407	609	982	284	839
Co		14	7	5	4	6	24	9	0	47	16	9	0	0	0	0	0
As		81	45	8	75	25	105	31	33	128	0	0	79	66	144	25	30
Cd		22	5	8	5	8	2	3	0	5	1	1	6	9	2	4	1
Cl		214087	221622	201365	210441	325232	203171	329314	298011	25970	20907	169915	203802	264179	181395	169734	175510
Br		348	602	226	149		107	345	181	121	165	175	251			239	210
Sulfate		1598	3008	1170	4194	17	3303	2474		606	725	7384	1302	20638			11
Cl/Br		615	368	889	1408		1901	954	1647	2142	1270	973	811			711	836
+ve/-ve		1.41	1.33	1.48	1.33	1.34	1.38	1.53	1.57	1.07	1.19	1.35	1.26	1.05	1.08	1.20	1.23

Table 4: Representative results of analyses of fluid inclusion leachates from vein quartz. Fluid compositions were reconstructed by charge balance of total cations against Cl molality determined from microthermometric data (Allen et al., 2005).

Site	Kirunavaara			Nuktus		Pahtohavare			Nautanen			Aitik		
Sample	KR2.4	KR2.24	KR2.17	NK2.1	NK2.3	PAH 8.14	PAH 8.20	PAH 8.9	NAU 7706e.1	NAU 7706e.2	NAU 7706t.1	A3a.1	A3.10	A3.17
Type	1	1	1	1	1	2	2	2	3	4	1	1	1	4
Salinity (wt. % NaCl eq.)	34.6	32.7	32.7	34.9	34.9	53.3	45.2	51.3	13.8	13.7	33.7	28.2	29.3	21.0
Na	110504	210340	91938	73653	184307	25816	287257	201447	54430	33245	110369	17031	189525	132340
K	72248			5720	63180			15498	20579	24209	28895	7744		
Na/K	2			13	3			13	3	1	4			
Ca	11682							9505	13476	17229	62346	138540		
Na/Ca	9			60834	2204			21	4	2	2			
Mg	28005			1	84				1392	4631	9275	51		
Ba	5088			1289	1617			1227	368	95	237	1571		
Mn				27598	233			5187			268	265		
Fe	2373			67701	1550			129164	3612	9442	1073	960		
Cu		480	252			83	2297		901	711	163	17	335	5182
Zn									761	5548	109	192		
Ag		10					8337		520	487	87	bd	11	102
Au		5					58						30	6
Pb		5358					2494		805	617	160	12	266	221
B			423			31								
Cl			198458			323220								
Br			1961			8119								

1. Lw+Sh+V; 2. Lw+nS+V; 3. Lw+V; 4. Lw+Lc+V

Table 5: Representative examples of LA-ICPMS analyses of fluid inclusions. Compositions are shown in ppm as either total cations charge balanced against Cl molality from microthermometry (Allen et al., 2005) or normalised to Cl concentration in ppm where the major cations had not been analysed.

	KR2						N2.5						PAH88217					
	Crush -Leach	LA-ICPMS mean	30% RSD	*n*	*min*	*max*	Crush -Leach	LA-ICPMS mean	30% RSD	*n*	*min*	*max*	Crush -Leach	LA-ICPMS mean	30% RSD	*n*	*min*	*max*
Na	92202	89865	26960	*15*	*44230*	*139972*	120353	139282	41785	*8*	*24140*	*195543*	227301	173263	51979	*22*	*12141*	*343311*
K	23051	91107	27332	*15*	*35434*	*130390*	31150	42940	12882	*8*	*4260*	*147576*		31397	9419	*13*	*4466*	*82450*
Li	204						241											
Ca	67835	10916	3275	*15*	*2274*	*34627*	53805	34487	10346	*8*	*2204*	*160665*	63228	43532	13060	*13*	*6390*	*118877*
Fe	1317	2068	620	*15*	*160*	*6225*	5380	20134	6040	*8*	*1550*	*67701*	24171	131303	39391	*13*	*25850*	*284514*
Mn	5809						3058	5120	1536	*8*	*232*	*27598*	7779	12011	3603	*13*	*1063*	*30996*
Pb	909	2779	834	*6*	*432*	*5358*	1076						422	843	253	*5*	*8*	*2494*
Zn	3497						2039						1729					
Sr	3444						2138						1377					
Ba	10867	4325	1298	*15*	*348*	*8858*	10407	3055	917	*8*	*1289*	*6046*	4466	2315	695	*13*	*127*	*4503*
Al	448						227						1681					
Cu	145	558	167	*13*	*36*	*3268*	92						128	2266	680	*9*	*1*	*2297*
B	586	237	71	*7*	*35*	*423*	177						128	664	199	*2*	*31*	*1298*
Co	5						14						6					
As	8						81						25					
Cd	8						22						8					
Cl	201365	191805	57542	7	*187644*	*198458*	214087						325232	314187	94256	*4*	*304026*	*325479*
Br	226	2484	745	6	*186*	*1961*	348							7609	2283	*4*	*2967*	*16014*
Sulfate	1170						1598						17					

Table 6: Comparison of reconstructed fluid composition from crush-leach analyses with mean reconstructed fluid inclusion composition from LA-ICPMS analyses. All concentrations in ppm.

Figure(s)

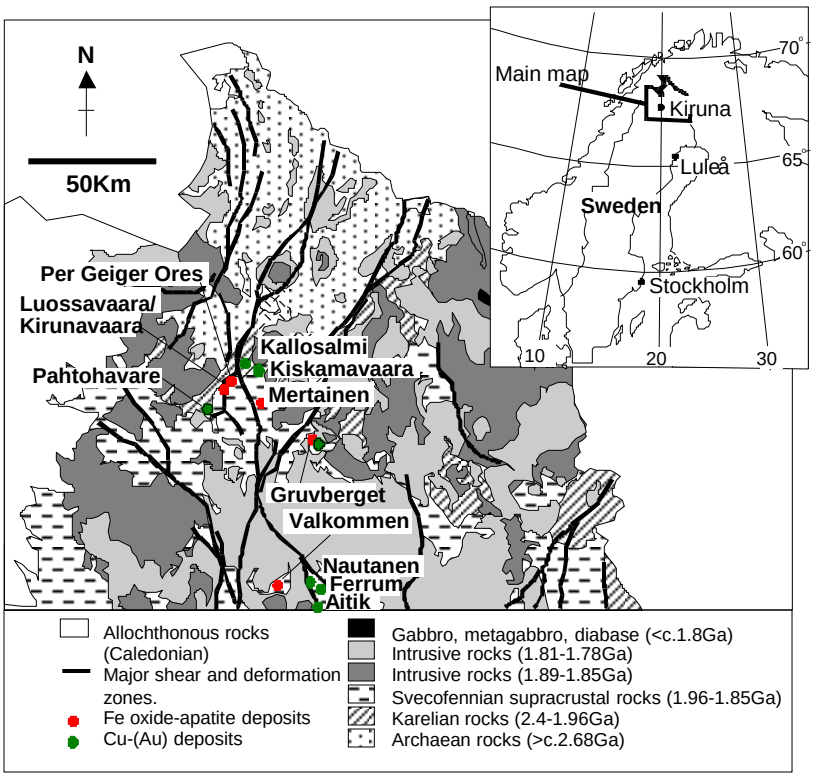
N
50Km
Per Geiger Ores
Luossavaara/
Kirunavaara
Pahtohavare
Kallosalmi
Kiskamavaara
Mertainen
Gruvberget
Valkommen
Nautanen
Ferrum
Aitik
Main map
Kiruna
Luleå
Sweden
Stockholm
70°
65°
60°
10
20
30
Allochthonous rocks (Caledonian)
Major shear and deformation zones.
Fe oxide-apatite deposits
Cu-(Au) deposits
Gabbro, metagabbro, diabase (<c.1.8Ga)
Intrusive rocks (1.81-1.78Ga)
Intrusive rocks (1.89-1.85Ga)
Svecofennian supracrustal rocks (1.96-1.85Ga)
Karelian rocks (2.4-1.96Ga)
Archaean rocks (>c.2.68Ga)

Figure(s)

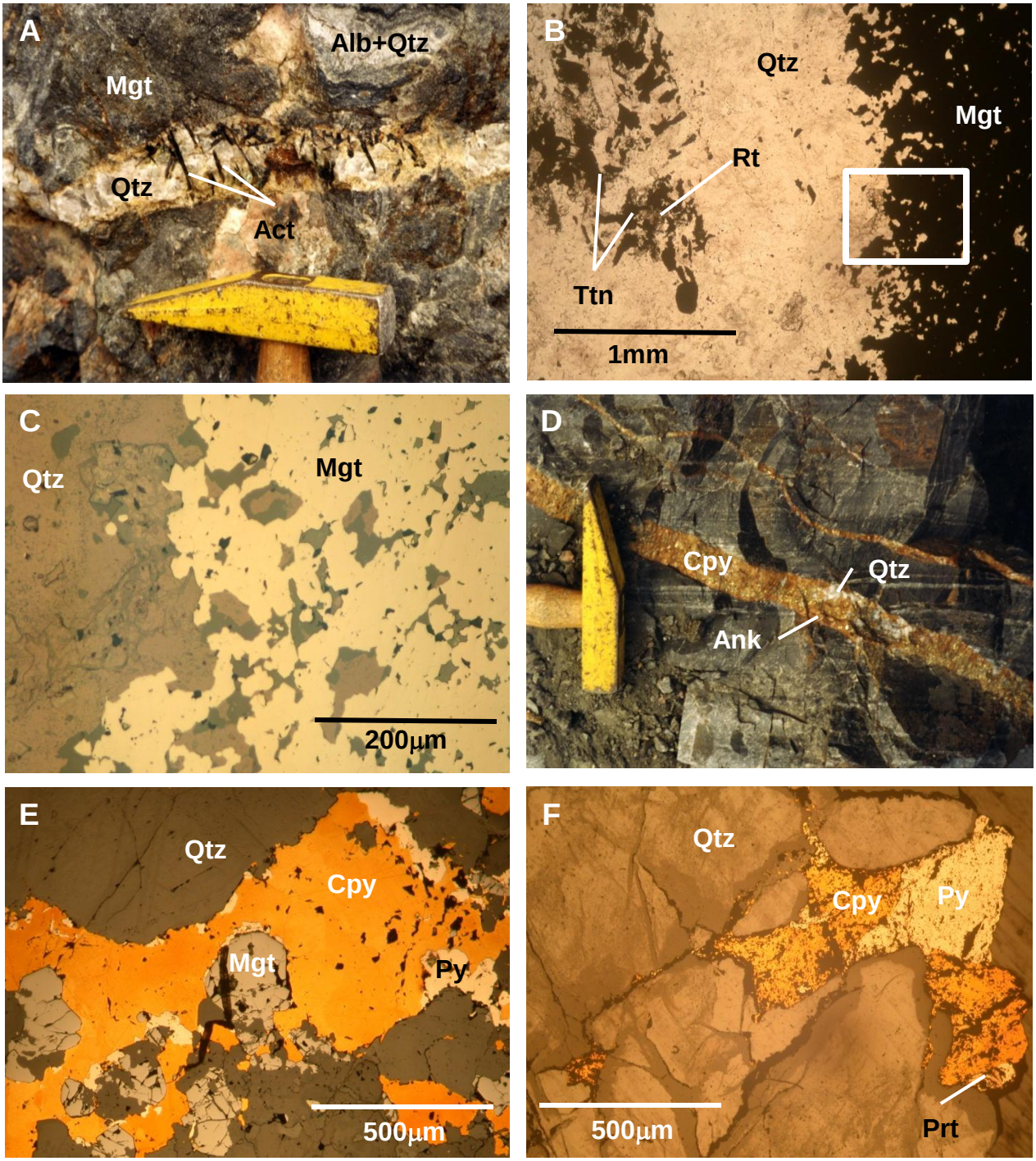
A
Alb+Qtz
Mgt
Qtz
Act
B
Qtz
Mgt
Rt
Ttn
1mm
C
Qtz
Mgt
200μm
D
Cpy
Qtz
Ank
E
Qtz
Cpy
Mgt
Py
500μm
F
Qtz
Cpy
Py
500μm
Prt

Figure(s)

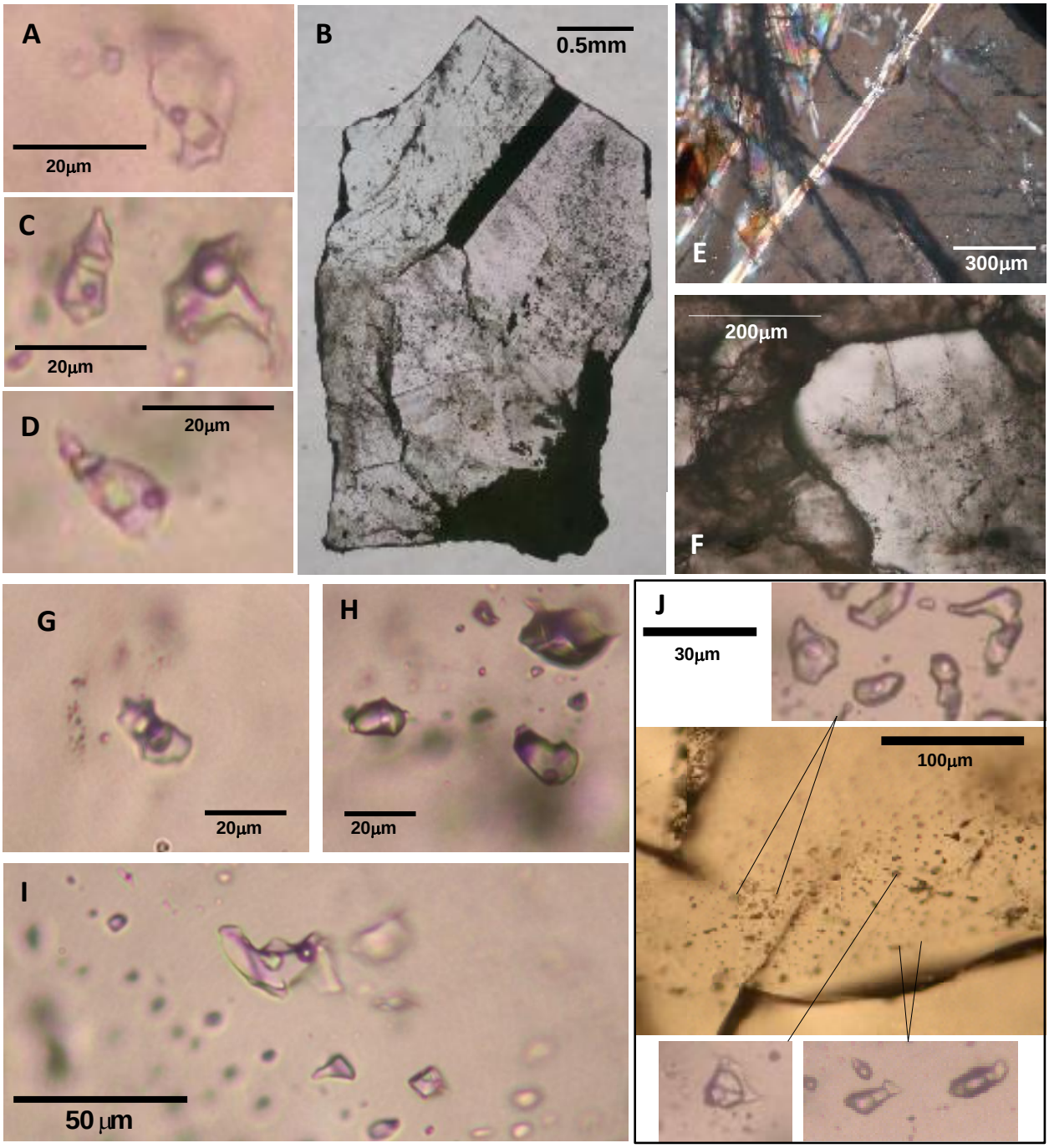
A
20μm
B
0.5mm
C
20μm
D
20μm
E
300μm
200μm
F
G
20μm
H
20μm
J
30μm
100μm
I
50 μm

Figure(s)

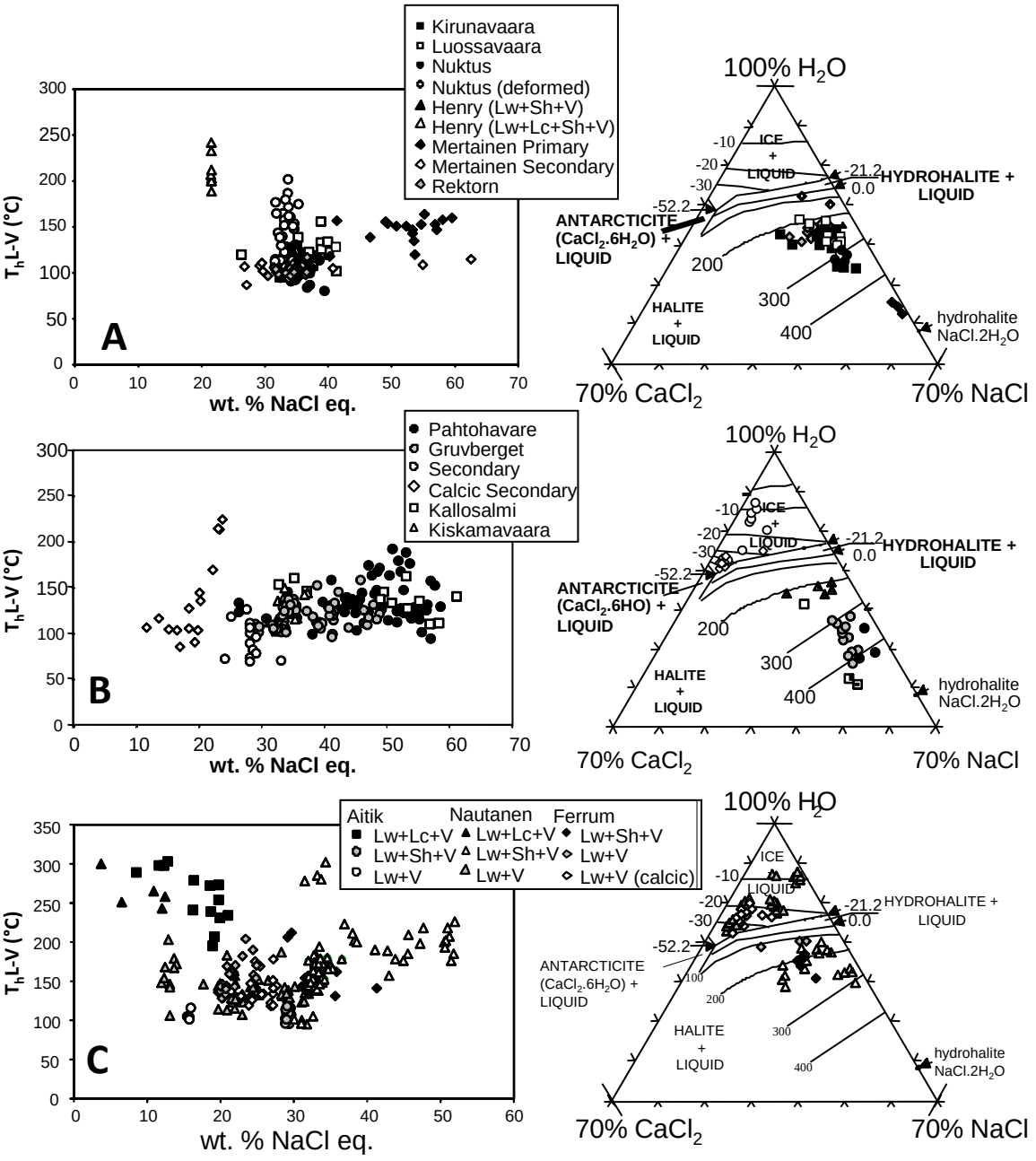
Kirunavaara
Luossavaara
Nuktus
Nuktus (deformed)
Henry (Lw+Sh+V)
Henry (Lw+Lc+Sh+V)
Mertainen Primary
Mertainen Secondary
Rektorn
A
T_hL-V (°C)
wt. % NaCl eq.
100% H_2O
ICE + LIQUID
HYDROHALITE + LIQUID
ANTARCTICITE ($CaCl_2.6H_2O$) + LIQUID
HALITE + LIQUID
hydrohalite $NaCl.2H_2O$
70% $CaCl_2$
70% NaCl
Pahtohavare
Gruvberget
Secondary
Calcic Secondary
Kallosalmi
Kiskamavaara
B
Aitik
Nautanen
Ferrum
Lw+Lc+V
Lw+Sh+V
Lw+V
Lw+Lc+V
Lw+Sh+V
Lw+V
Lw+Sh+V
Lw+V
Lw+V (calcic)
C

Figure(s)

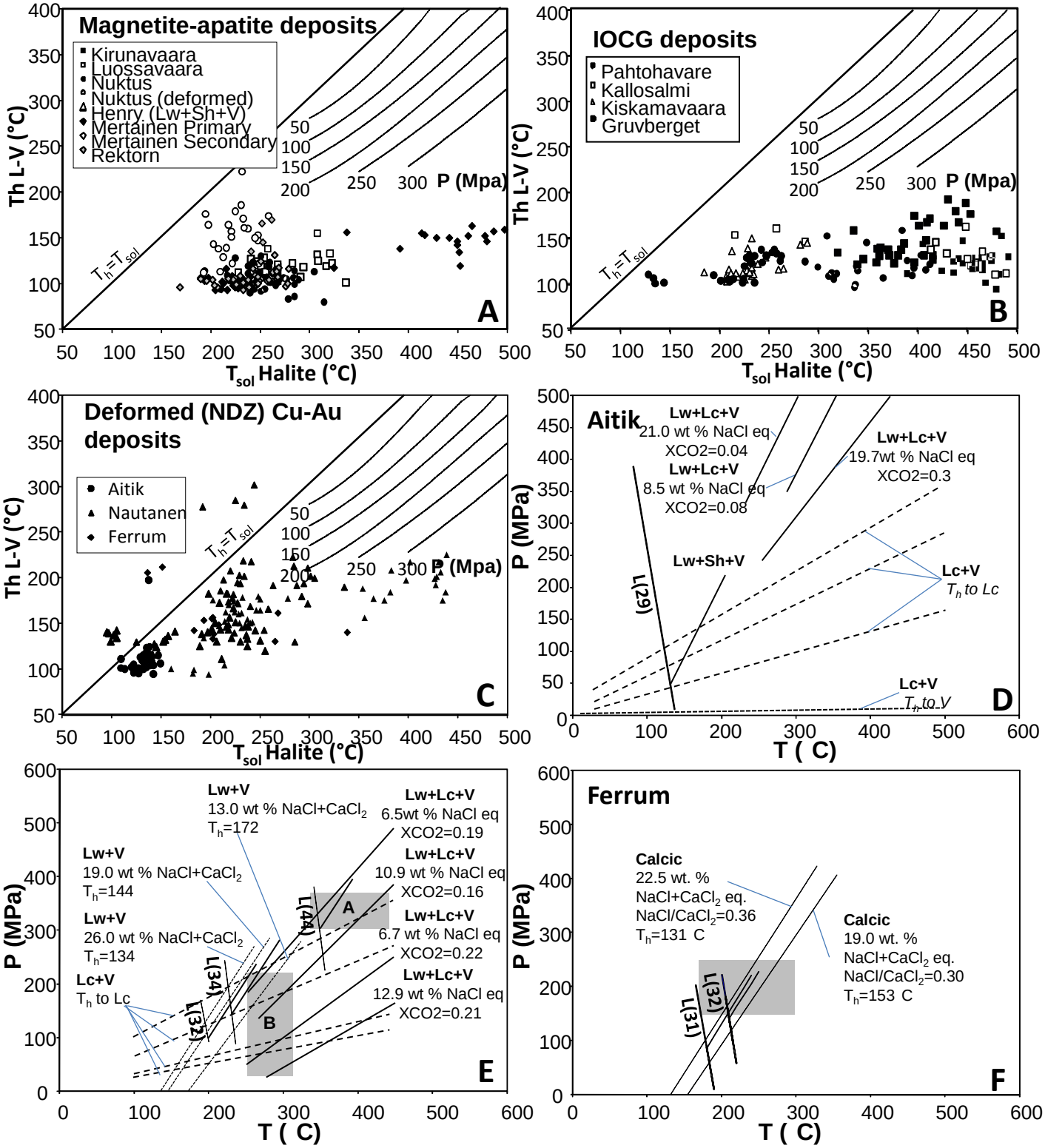
Magnetite-apatite deposits
Kirunavaara
Luossavaara
Nuktus
Nuktus (deformed)
Henry (Lw+Sh+V)
Mertainen Primary
Mertainen Secondary
Rektorn
50
100
150
200
250
300
P (Mpa)
Th=Tsol
Th L-V (°C)
Tsol Halite (°C)
A
IOCG deposits
Pahtohavare
Kallosalmi
Kiskamavaara
Gruvberget
B
Deformed (NDZ) Cu-Au deposits
Aitik
Nautanen
Ferrum
C
Aitik
Lw+Lc+V
21.0 wt % NaCl eq
XCO2=0.04
Lw+Lc+V
8.5 wt % NaCl eq
XCO2=0.08
Lw+Lc+V
19.7wt % NaCl eq
XCO2=0.3
Lw+Sh+V
L(29)
Lc+V
Th to Lc
Lc+V
Th to V
P (MPa)
T (C)
D
Lw+V
13.0 wt % NaCl+CaCl2
Th=172
Lw+V
19.0 wt % NaCl+CaCl2
Th=144
Lw+V
26.0 wt % NaCl+CaCl2
Th=134
Lc+V
Th to Lc
Lw+Lc+V
6.5wt % NaCl eq
XCO2=0.19
Lw+Lc+V
10.9 wt % NaCl eq
XCO2=0.16
Lw+Lc+V
6.7 wt % NaCl eq
XCO2=0.22
Lw+Lc+V
12.9 wt % NaCl eq
XCO2=0.21
L(44)
L(43)
L(42)
L(32)
A
B
E
Ferrum
Calcic
22.5 wt. %
NaCl+CaCl2 eq.
NaCl/CaCl2=0.36
Th=131 C
Calcic
19.0 wt. %
NaCl+CaCl2 eq.
NaCl/CaCl2=0.30
Th=153 C
L(32)
L(31)
F

Figure(s)

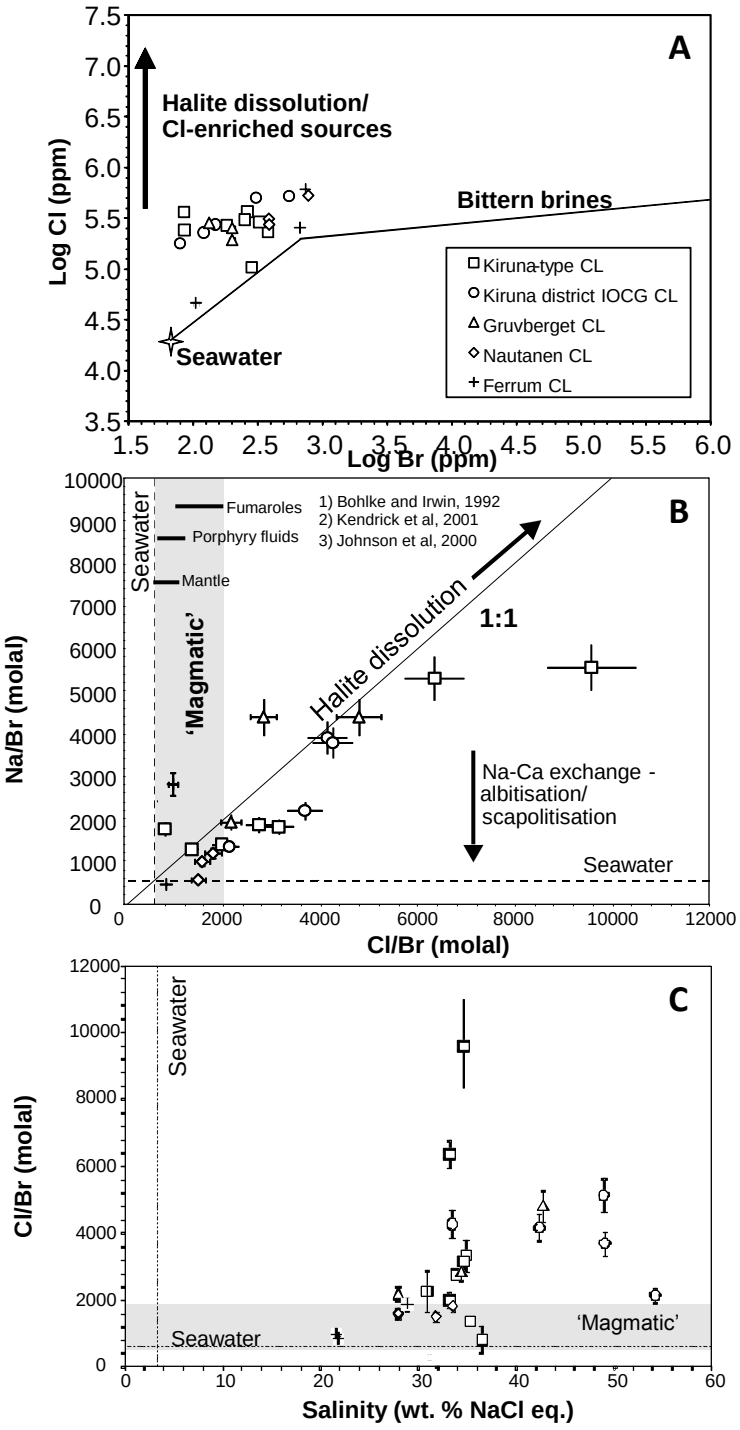
A
Halite dissolution/
Cl-enriched sources
Bittern brines
Seawater
Kiruna-type CL
Kiruna district IOCG CL
Gruvberget CL
Nautanen CL
Ferrum CL
Log Cl (ppm)
Log Br (ppm)
B
Seawater
Fumaroles
Porphyry fluids
Mantle
'Magmatic'
1) Bohlke and Irwin, 1992
2) Kendrick et al, 2001
3) Johnson et al, 2000
Halite dissolution
1:1
Na-Ca exchange - albitisation/ scapolitisation
Seawater
Na/Br (molal)
Cl/Br (molal)
C
Seawater
'Magmatic'
Seawater
Cl/Br (molal)
Salinity (wt. % NaCl eq.)

Figure(s)

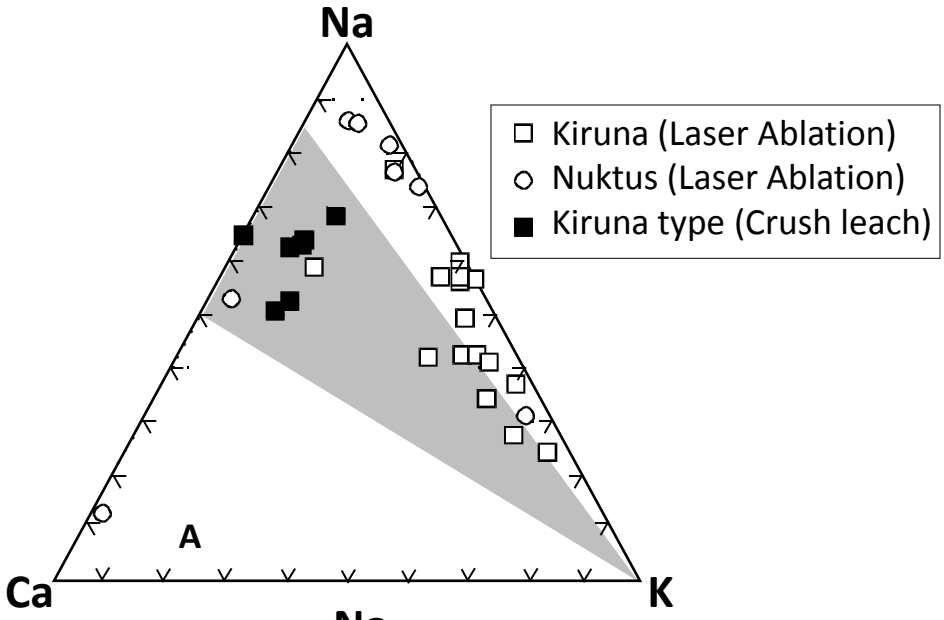
Na
Ca
K
A
Kiruna (Laser Ablation)
Nuktus (Laser Ablation)
Kiruna type (Crush leach)

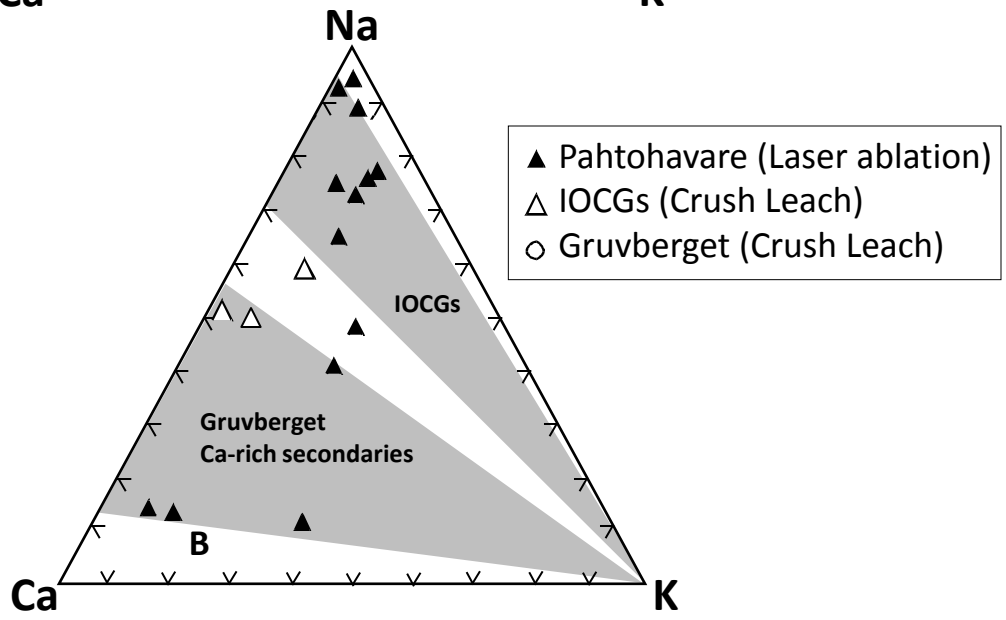
Na
Ca
K
B
IOCGs
Gruvberget
Ca-rich secondaries
Pahtohavare (Laser ablation)
IOCGs (Crush Leach)
Gruvberget (Crush Leach)

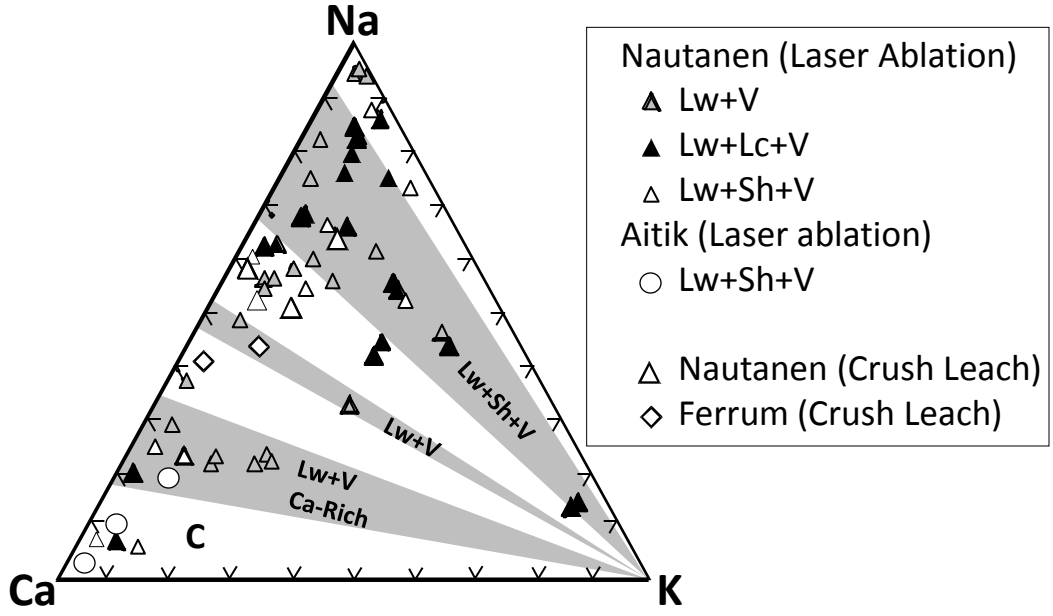
Na
Ca
K
C
Lw+Sh+V
Lw+V
Lw+V
Ca-Rich
Nautanen (Laser Ablation)
Lw+V
Lw+Lc+V
Lw+Sh+V
Aitik (Laser ablation)
Lw+Sh+V
Nautanen (Crush Leach)
Ferrum (Crush Leach)

Figure(s)

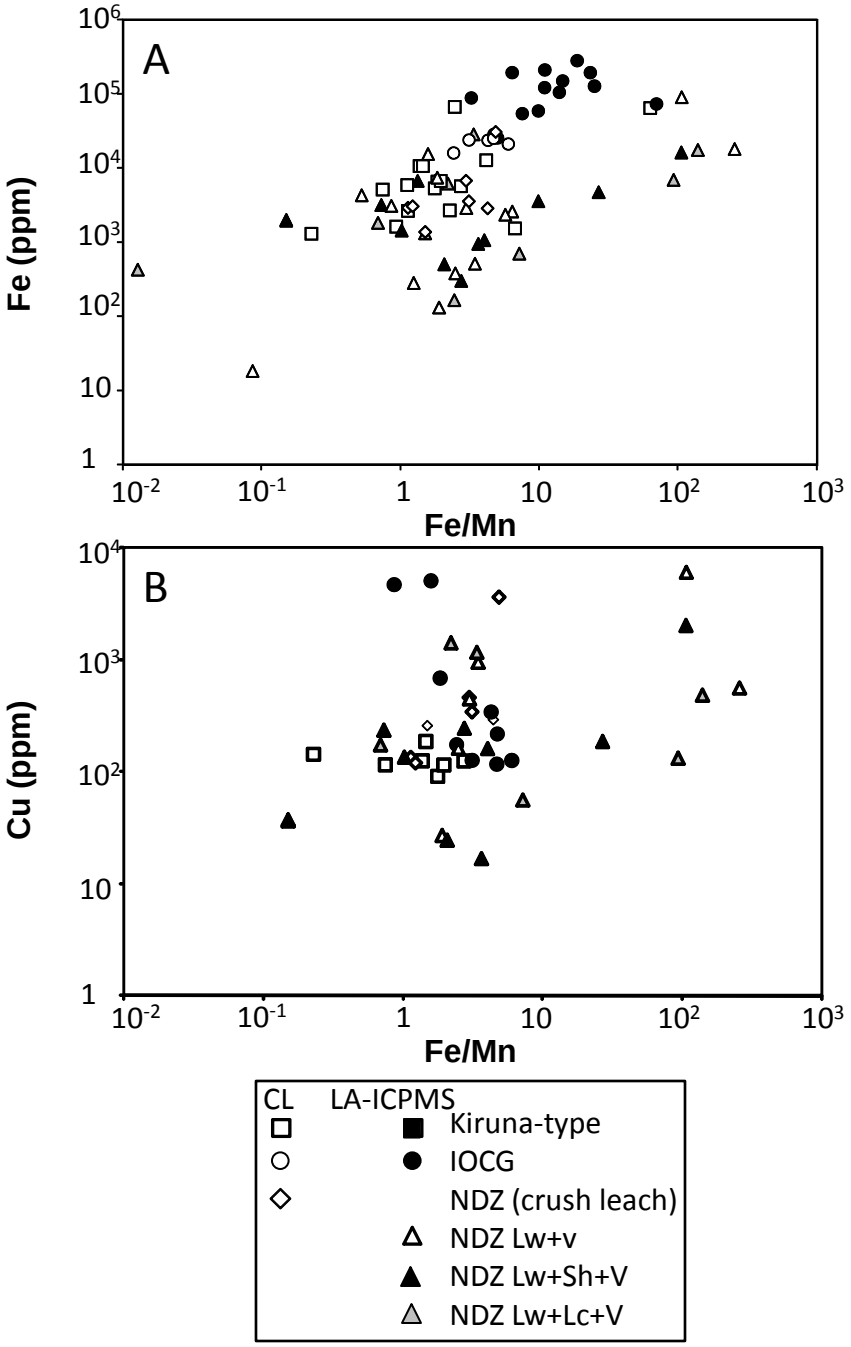
A
B
Fe (ppm)
Cu (ppm)
Fe/Mn
Fe/Mn
CL
LA-ICPMS
Kiruna-type
IOCG
NDZ (crush leach)
NDZ Lw+v
NDZ Lw+Sh+V
NDZ Lw+Lc+V

Figure(s)

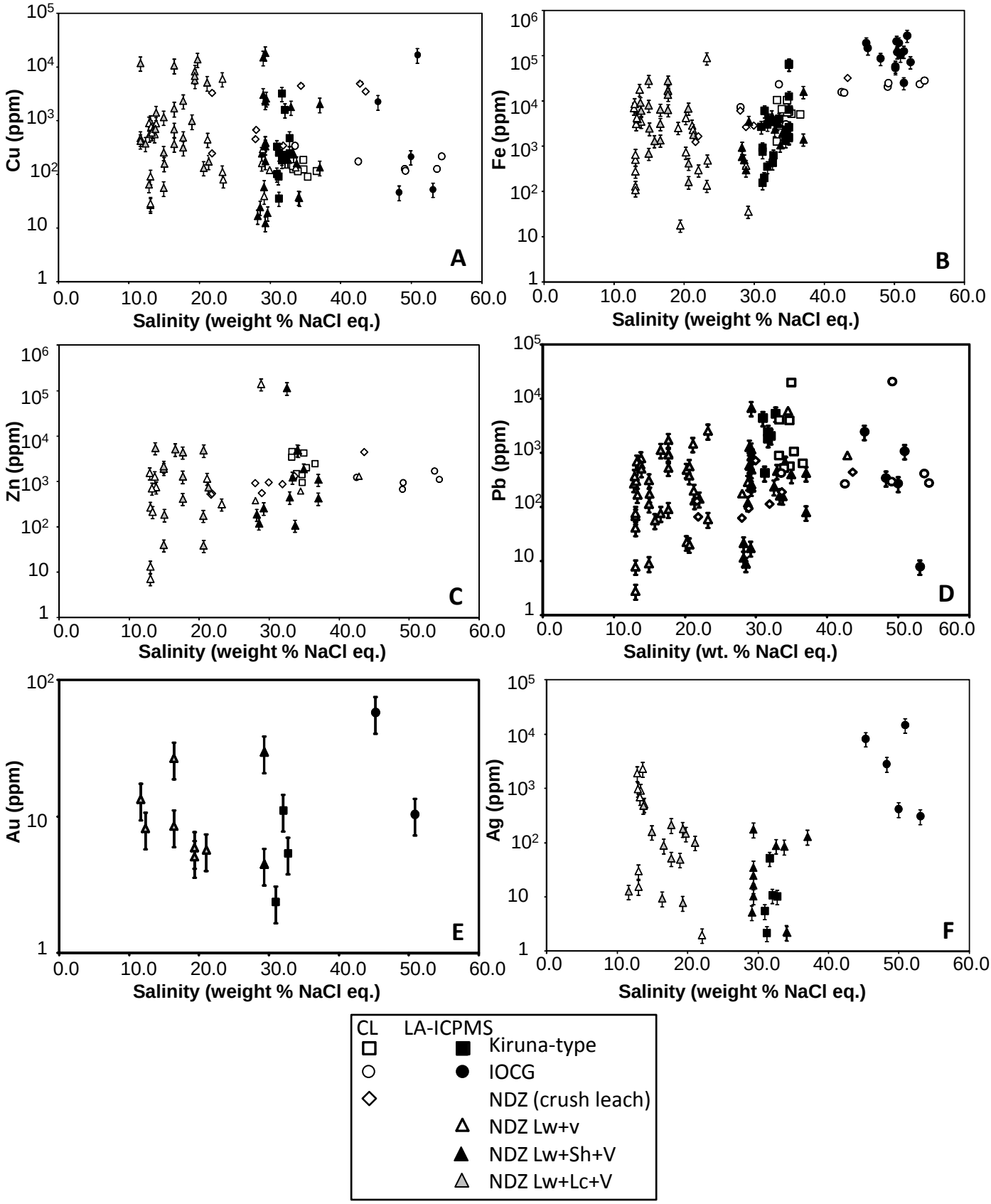
Cu (ppm)
Salinity (weight % NaCl eq.)
A
Fe (ppm)
Salinity (weight % NaCl eq.)
B
Zn (ppm)
Salinity (weight % NaCl eq.)
C
Pb (ppm)
Salinity (wt. % NaCl eq.)
D
Au (ppm)
Salinity (weight % NaCl eq.)
E
Ag (ppm)
Salinity (weight % NaCl eq.)
F
CL
LA-ICPMS
Kiruna-type
IOCG
NDZ (crush leach)
NDZ Lw+v
NDZ Lw+Sh+V
NDZ Lw+Lc+V

Figure(s)

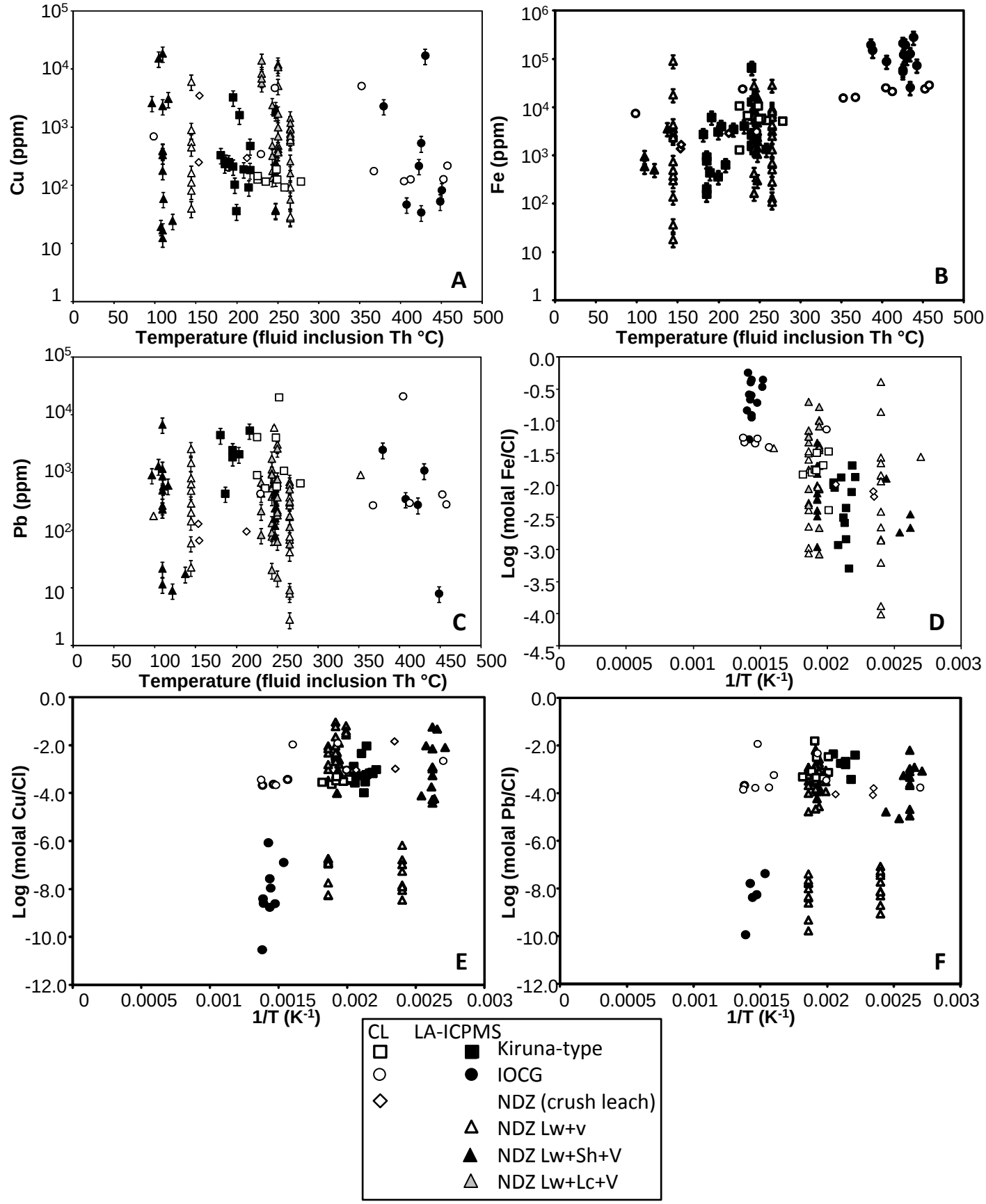
Cu (ppm)
Temperature (fluid inclusion Th °C)
A
Fe (ppm)
Temperature (fluid inclusion Th °C)
B
Pb (ppm)
Temperature (fluid inclusion Th °C)
C
Log (molal Fe/Cl)
1/T (K-1)
D
Log (molal Cu/Cl)
1/T (K-1)
E
Log (molal Pb/Cl)
1/T (K-1)
F
CL
LA-ICPMS
Kiruna-type
IOCG
NDZ (crush leach)
NDZ Lw+v
NDZ Lw+Sh+V
NDZ Lw+Lc+V

Figure(s)

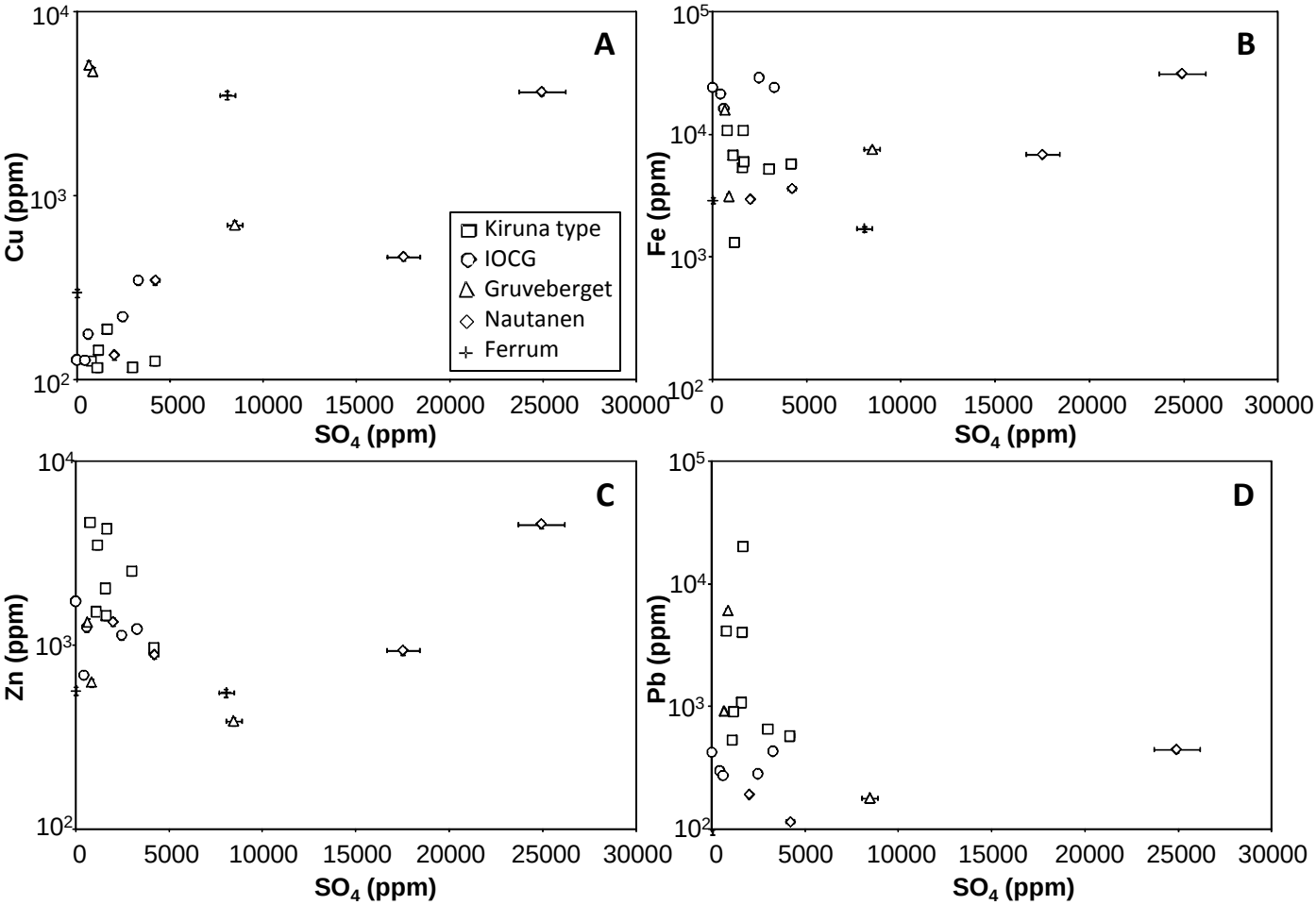
A
B
C
D
Cu (ppm)
Fe (ppm)
Zn (ppm)
Pb (ppm)
SO4 (ppm)
Kiruna type
IOCG
Gruveberget
Nautanen
Ferrum